56p

ORNL-3505
UC-34 – Physics
TID-4500 (27th ed.)

MEASUREMENT OF THE INTENSITY OF THE PROTON BEAM OF THE HARVARD UNIVERSITY SYNCHROCYCLOTRON FOR ENERGY-SPECTRAL MEASUREMENTS OF NUCLEAR SECONDARIES

R. T. Santoro [redacted]
R. W. Peelle

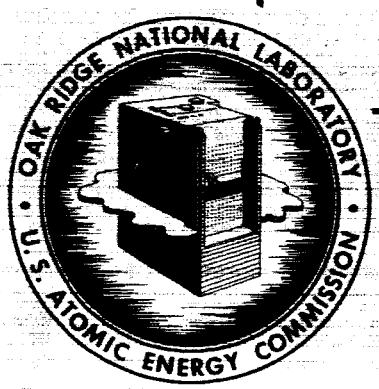

OAK RIDGE NATIONAL LABORATORY
operated by
UNION CARBIDE CORPORATION
for the
U.S. ATOMIC ENERGY COMMISSION

(NASA CR-- ; ORNL- 3505) OTS:
(not for sale on front cover)

(Contract No. W-7405-eng-26)

Neutron Physics Division

MEASUREMENT OF THE INTENSITY OF THE PROTON BEAM OF THE HARVARD UNIVERSITY SYNCHROCYCLOTRON FOR ENERGY-SPECTRAL MEASUREMENTS OF NUCLEAR SECONDARIES *

R. T. Santoro and R. W. Peelle **a

MARCH 1964 86 p refer

*Work performed under (NASA Order Nos. T-7632 and R-104); NASA order
**Wrote Section VIII and assisted materially in the conduct of the experiments and the preparation of this report.

support code
2

OAK RIDGE NATIONAL LABORATORY
Oak Ridge, Tennessee
operated by
UNION CARBIDE NUCLEAR COMPANY
for the
U.S. ATOMIC ENERGY COMMISSION

1763192

18427

Abstract

A

Two thin helium-filled parallel-plate ionization chambers were designed for use in continuously monitoring the 160-MeV proton beam of the Harvard University Synchrocyclotron over an intensity range from 10^5 to 10^{10} protons/sec. The data were required for support of various measurements of energy spectra of neutrons, protons, and gamma rays resulting from the interaction of high-energy protons with various targets representative of typical space vehicle shielding materials.

The ionization chambers were calibrated by two independent methods. In four calibrations the charge collected in the ionization chambers was compared with that deposited in a Faraday cup which followed the ionization chambers in the proton beam. In a second method, a calibration was made by individually counting beam protons with a pair of thin scintillation detectors. The ionization chamber response was found to be flat within 2% for a five-decade range of beam intensity.

Comparison of the Faraday-cup calibrations with that from proton counting shows agreement to within 5%, which is considered satisfactory for the purposes to which the data will be put. The experimental results were also in agreement, within estimated errors, with the ionization chamber response calculated using an accepted value of the average energy loss per ion pair for helium. A slow shift in the calibrations with time is ascribed to a gradual contamination of the helium of the chambers by air leakage.

An appendix describes the calibration of standard current sources used for accurate calibration of the current-measuring instruments.

Author

Table of Contents

I. Introduction

In October of 1962 measurements of the energy spectra of the neutrons, protons, and gamma rays resulting from the interactions of 160-MeV protons with various targets[1] were carried out by ORNL Neutron Physics Division personnel at the Harvard University Synchrocyclotron. The work was part of a continuing effort to provide experimental data against which calculations of spacecraft shielding may be compared. These experiments required that the intensity of the proton beam be continuously measured over a range of 10^5 to 10^{10} protons/sec by a method such that the energy of the beam striking the target would not be greatly degraded. This paper discusses the choice of a monitor, its design, and the results of calibrations by two independent methods.

II. Selection of the Monitoring System

The optimum device for measurement of cyclotron proton beam intensity is generally accepted[2] to be the Faraday cup, a heavy metallic block which measures the intensity as a function of the charge transferred by the beam protons. Since the nature of the experiments required continuous monitoring, this device could not be used. The targets were of sufficient thickness (1.2 times the proton range) to act as complete absorbers, so that a Faraday cup could not be used following the target, and since the cup is also a total absorber, it obviously could not precede the target in the beam.

The criteria of continuous monitoring, linear response over a wide range of beam intensities, and minimum attenuation of the beam in energy and intensity eliminated from consideration such possible monitors as foils, scintillation detectors, and counter telescopes. Within the criteria noted above, the most obvious choice for the beam monitor was an ionization chamber. Although some other low-attenuating devices, such as beam induction electrodes and secondary emission monitors, were not considered in making this choice there is presently no reason to believe that they would have performed more satisfactorily than did the ionization chambers.

---

1. Section 9, Vol. II, Neutron Phys. Div. Ann. Progr. Rept., Aug. 1, 1963, ORNL-3499, p 63, ff.
2. D. M. Ritson, Chap. XI, Vol. 5 of Techniques of High-Energy Physics, Interscience, New York, 1961.

III. Design of Ionization Chambers

A primary requirement in the use of ionization chambers for proton beam monitoring was that the chamber response be flat over the range from 10^5 to 10^{10} protons/sec. In preliminary experiments the responses of three different types of chambers were tested. One was a free-air chamber,[3] and two were parallel-plate chambers,[4] one filled with nitrogen and the other with helium. A comparison of the responses of the three is shown in Fig. 1. The air-filled and nitrogen-filled chambers are clearly unsatisfactory, while the helium-filled chamber appears to be nearly optimum except for its comparatively low efficiency. It was therefore decided to adopt the basic design of the helium-filled chamber, making changes to improve collection efficiency by reducing the rate of recombination and to better know the gas pressure and electrode spacing.

Two helium-filled parallel-plate ionization chambers were built[5] according to the design shown in Fig. 2. The chambers differ from those of Koehler in their sensitive volume, which was increased from 115.8 cm^3 to 205.9 cm^3 by increasing the electrode diameter from 7.62 cm to 10.16 cm, and in the fact that they have five electrodes rather than the three of the original design. The overall space occupied by the electrodes remains at 2.54 cm. These changes increased the surface-to-volume ratio by a factor of two.

The electrodes consist of aluminized mylar having a nominal areal density of 1 mg/cm^2. The windows are 2-mil-thick aluminum foil. Total material in the beam is 32.6 mg/cm^2, which corresponds to an energy loss of 135 keV for 160-MeV protons. Current leakage was minimized by selecting connectors having leakage resistances greater than 10^{14} Ω and by using a guard ring around the collector connector.

The ionization chambers were filled with helium to a pressure of 73 cm Hg at 23°C. The gas was flowed directly from a commercially bottled

3. Designed and built by W. A. Gibson, Neutron Physics Division, ORNL.
4. Designed and built by Dr. A. M. Koehler of the Harvard University staff, who loaned them, along with a Faraday cup, for these preliminary tests.
5. Built by R. K. Abele, Instrumentation and Controls Division. Construction details are given in Drawing Q-2540.

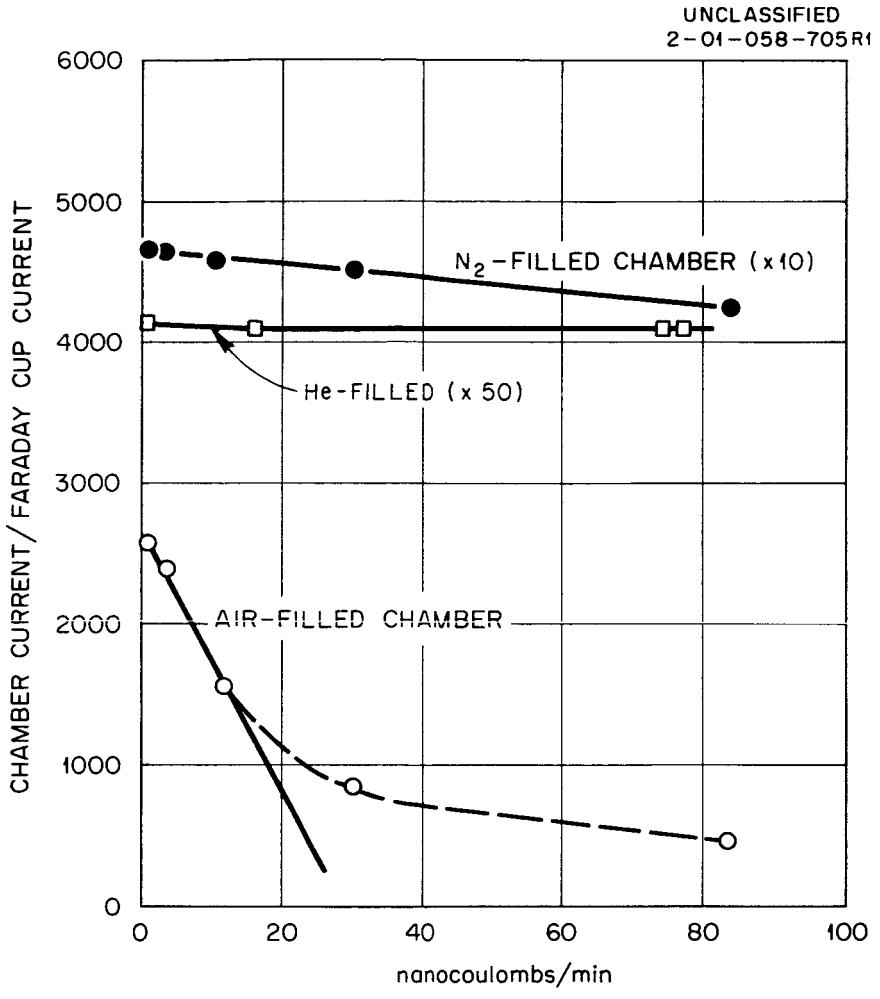

Fig. 1. Comparison of Ion Chamber Performances. The ordinates of the points plotted for the N_2-filled chamber have been multiplied by 10; those for the He-filled chamber have been multiplied by 50.

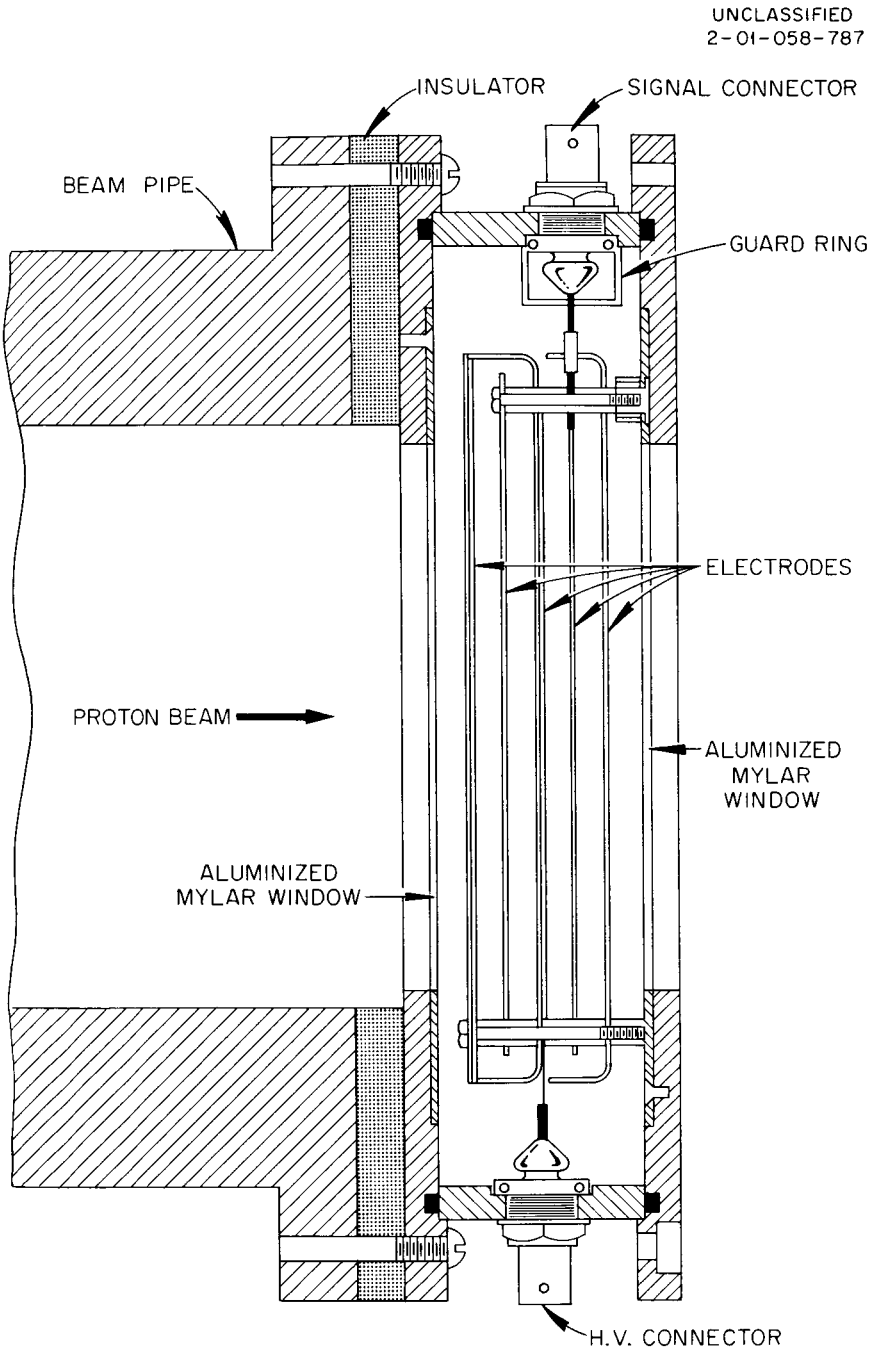

Fig. 2. Cross Section of Parallel-Plate Ionization Chamber.

supply, with no regard for the possible fraction of contaminants. It was assumed that the helium was at least 98% pure.

By making the (rather broad) assumption that the mobility of the ions, the ionization intensity, the voltage between the plates, the collection efficiency, and the gas pressure are the same for both the Koehler chamber and the present version, the recombination, to a first approximation, is given by $R = Ad^4$, where A is a constant which includes the effects noted above and d is the plate separation in cm. This follows from the equation given by Boag,[6] in which R is shown to vary as d^5. Thus changing the number of electrodes from three to five theoretically reduces the total recombination by a factor of 16.

Typical saturation curves for the redesigned chambers are shown in Fig. 3. These data show the ratio of the current collected by the ionization chambers to that collected by a Faraday cup, as a function of voltage and for a constant beam intensity of 1.84×10^{10} protons/sec, which was within the region of maximum beam intensity to be used for the spectral measurements. From these data the chamber operating voltage was chosen to be 300 V for all experiments.

The response of the ion chambers to 160-MeV protons, in ion pairs/proton, can be computed from

$$\text{ip/proton} = (dE/dx)\, W^{-1}\, d_t \rho \ , \qquad (1)$$

where

$dE/dx = (5.15 \pm 0.26) \times 10^6$ eV·cm^2·g^{-1}·proton^{-1} (Ref. 7),

W = the mean energy expended in the production of an ion pair in helium (eV/ip),

d_t = overall space occupied by electrodes, 2.54 cm,

ρ = helium density, 0.178×10^{-3} g/cm^3.

---

6. J. W. Boag, p 165 in Radiation Dosimetry (ed. by G. J. Hine and G. L. Brownell), Academic, New York, 1956.

7. K. B. Mather and P. Swan, Nuclear Scattering, Cambridge University Press, London, 1946, p 83.

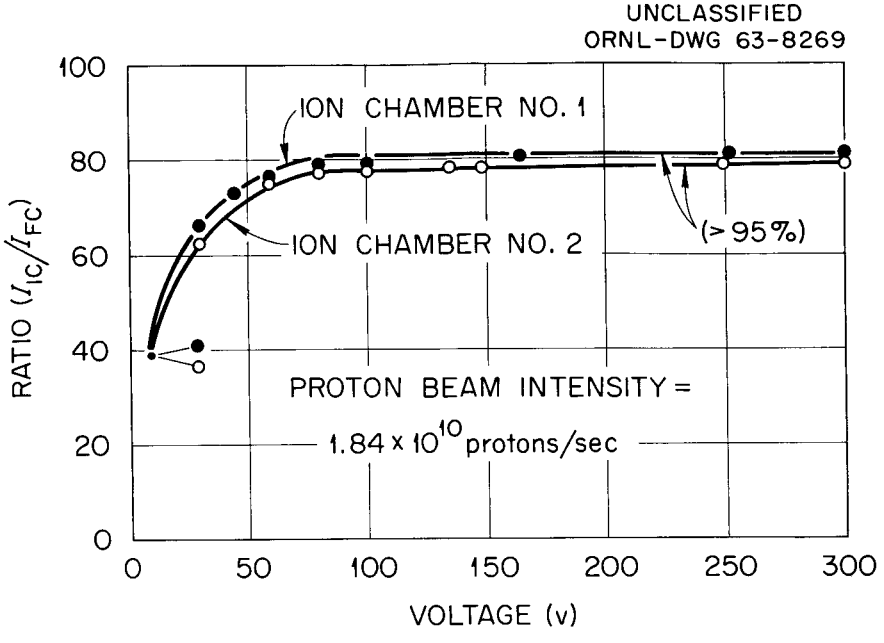

Fig. 3. Ionization Chamber Saturation Curves.

The calculated value for the response of the chambers is 80.4 ± 2.8 ion pairs per normally incident proton. The error (3.4%) stems from an uncertainty in the value of W. Wilkinson[8] gives a value of 30 eV/ip, while Palevsky[9] gives a value of 28 eV/ip. The value used was 29, the average of the two quoted.

IV. Faraday Cup Design

Although the response of an ionization chamber may be calculated, as demonstrated above, in practice it is more desirable to calibrate the chambers against the response of an absolute monitor. In the present work two independent calibrations were made, the first with a Faraday cup especially constructed for this purpose and the second by individual-proton counting techniques.

The design of the Faraday cup, shown in Fig. 4, was based on procedures suggested by Brown and Tautfest[10] and comments by Chamberlain et al.[11] on the use of a Faraday cup for calibrating ionization chambers.

The cup consists of a 6-in.-diam, 8-in.-long copper cylinder having a 4-in.-diam, 6-in.-long re-entrant opening into which the proton beam is directed. The base of the cup is nominally 45.2 g/cm^2 in thickness, which is sufficient to completely stop the incident 160-MeV proton beam. The cup is mounted in a brass housing on Teflon rings, which serve to isolate it electrically.

The accuracy of a Faraday cup is dependent on the number of charged particles which scatter into or out of the cup. Backscattering losses were diminished by making the cup re-entrant, thus reducing the solid angle at the base of the cup subtended by its mouth. This angle is given by

---

8. D. H. Wilkinson, Ionization Chambers and Counters, Cambridge University Press, London, 1950, p 20.
9. H. H. Palevsky, Mineapolis-Honeywell Regulator Co. Technical Bulletin No. NER-1 (1954).
10. K. L. Brown and G. W. Tautfest, Rev. Sci. Instr. 27(9), 696 (1956).
11. O. Chamberlain, E. Segre, and C. Weigand, Phys. Rev. 83, 923 (1951).

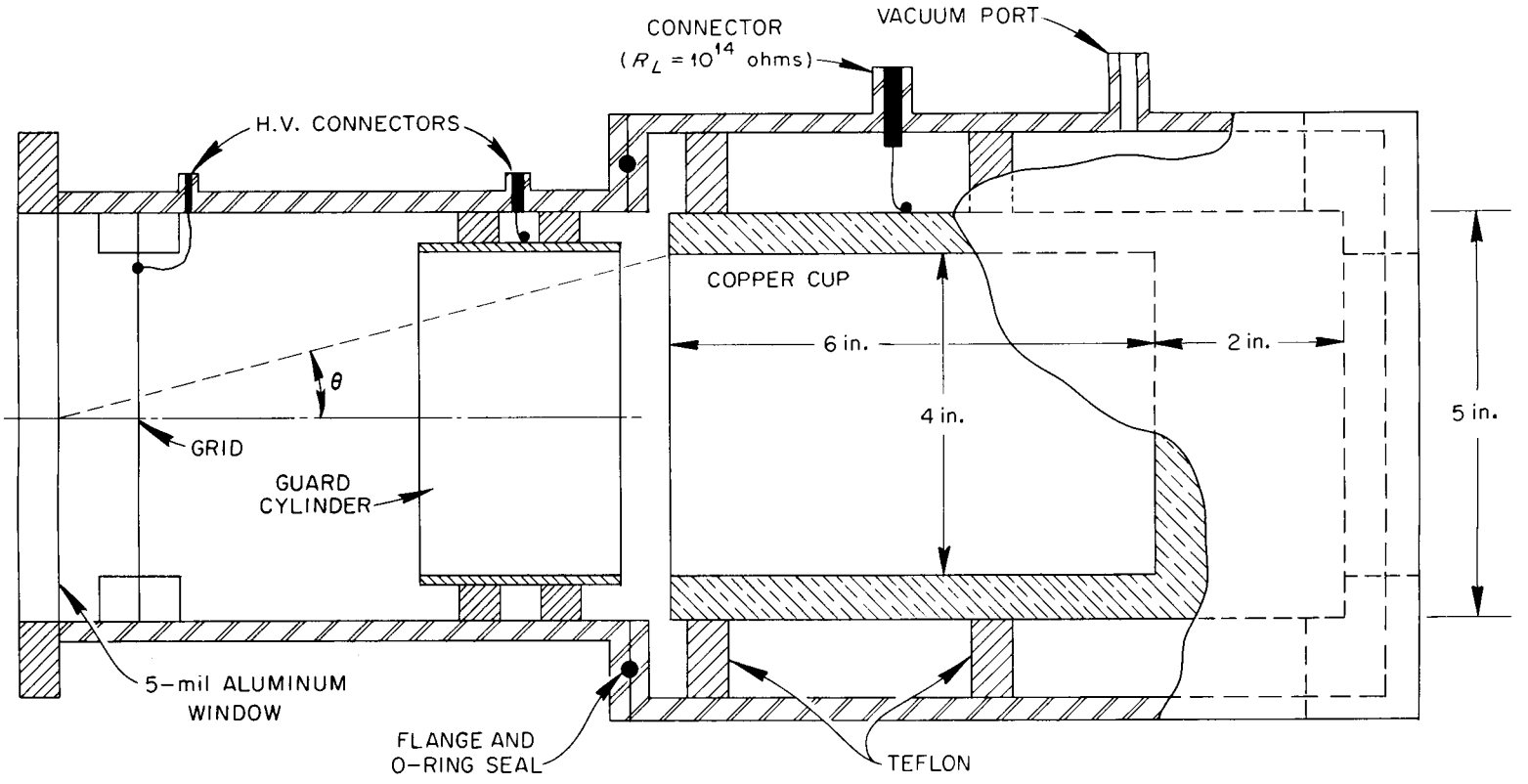

Fig. 4. Cross Section of Faraday Cup Assembly.

$$\frac{\Omega}{4\pi} = \frac{1}{2}\left[1 - \cos\left(\tan^{-1}\frac{d}{k}\right)\right] = 0.02566 \ , \qquad (2)$$

where d is the radius of the mouth and k is the depth of the mouth opening. In order to evaluate the accuracy of the cup, the fraction of charge lost due to escaping radiation and the effect of electrons entering the cup was estimated as detailed below.

Delta-Ray Escapes

Delta rays (electrons) are created by collisions of incident protons with atomic electrons of the cup. Symons[12] gives the cross section for proton-electron collisions as

$$d\sigma = \pi r_o^2 \frac{2m_e}{\beta^2} \frac{dE'}{(E')^2}\left[1 - \beta^2 \frac{E'}{E'_M} + \frac{1}{2}\left(\frac{E'}{E + m_p}\right)^2\right] \ , \qquad (3)$$

where

r_o = classical radius of the electron,

m_e = rest energy of the electron,

β = v/c, for the proton before collision,

E' = energy lost by the proton in the collision,

E = kinetic energy of the proton before collision,

m_p = rest energy of the proton,

E'_M = maximum E' allowed by conservation laws.

For the 160-MeV protons, the maximum energy attained by the secondary electron, E'_e, is given by

$$E'_e = 4(m_e/m_p)\, E = 340 \text{ keV}. \qquad (4)$$

The range of 340-keV electrons in copper is 156 mg/cm^2, or 0.0175 cm. If it is assumed that the average typical reaction occurs midway of the 156-mg/cm^2 thickness, then only those electrons backscattered with energies of 220 keV or greater can escape.

---

12. K. R. Symons, Fluctuations in Energy Lost by High-Energy Charged Particles in Passing Through Matter, Thesis, Harvard University (1948).

Integrating Eq. 3 from 220 keV to 340 keV [with the second term in the square brackets neglected since the value of $(E'/E + m_p)^2$ is very much less than unity when m_p = 938 MeV, E = 160 MeV, and E' = 340 kev] gives $\sigma = 3.76 \times 10^{-24}$ cm^2. F, the number of electron-producing collisions that occur in the 156-mg/cm^2 thickness, is given by $F = N_e\sigma$, where N_e is the number of electrons per cm^2, and from this it appears that 16% of the protons interact to create "escapable" electrons. (N_e for the 156-mg/cm^2 copper slab equals 4.31×10^{22} electrons/cm^2.) If the backscattering is overweighted by assuming that all of the electrons are scattered isotropically in 4π geometry, then from Eq. 2 the fraction of charged-particle loss is 0.004.

Other delta rays are produced by protons interacting with the 5-mil-thick aluminum window. These electrons may be scattered out of the window and into the cup. With the assumption that all reactions occur at the mid-plane of the foil, the "escapable" electrons are those with energies between 90 and 340 keV. From the equation given by Rossi,[13]

$$E'_M = 2m_e c^2 \cos^2\theta \left[\beta^2/(1 - \beta^2)\right] , \qquad (5)$$

it is evident that the kinetic energy of the secondary electron decreases with increasing angle of scatter. Because of the arrangement of the components within the brass housing, the cup is affected by only a portion of the scattered electrons, i.e., those scattered within the angle θ shown in Fig. 4 ($\cos\theta = 0.96$). From Eq. 5, the energies of these electrons, assuming that they are emitted in straight paths, range from 315 to 340 keV. By integrating Eq. 3 between these limits, we determine σ to be 0.179×10^{-24} cm^2. For the 5-mil-thick aluminum foil the value of N_e is 1.02×10^{22} electrons/cm^2, and from the relation $F = N_e\sigma$ the fraction of protons which interact to form electrons which can enter the cup is 0.0018. The electrons scattered at angles greater than $\cos^{-1}$ 0.96 are assumed to have no effect upon the cup.

---

13. B. Rossi, High-Energy Particles, Prentice-Hall, New York, 1952.

Compton Electron Production in the Cup

Protons striking the cup may also give rise to gamma rays which in turn produce electrons through Compton reactions. If the gamma rays are predominantly forwardly scattered and the resultant electrons similarly scattered, then, depending upon the electron energies and point of origin, a fraction can escape through the base of the cup. If it is assumed that each proton interacts to form a 3-MeV gamma ray which in turn produces a 2-MeV electron, the electrons which escape are those born in the last 1.7 mm of copper, and their number is given by

$$(I_o\, e^{-\mu x}) \int_0^{0.17} \mu\, e^{-\mu t}\, dt\, P_e \,, \qquad (6)$$

where

P_e = probability that an electron born in this region escapes (assumed to be 1/2),

$\mu = 0.311\ cm^{-1}$.

The first term gives the intensity of the gamma ray at a point 4.90 cm from the base of the cup and is equal to 0.22. The integral term defines the rate of birth of the electrons in the last 1.7 mm of copper. The value of this integral is 0.05. The fraction of electrons which escape is therefore 0.005.

If it is assumed that the gamma rays are created at a depth of 1.27 cm in the base of the cup, rather than at the base as assumed above, and if the angular distribution of the gamma rays is isotropic, then the fraction of electrons which escape is reduced. However, those electrons which escape through the sides of the cup must also be considered. Considering all possibilities, the fraction of electrons escaping from the cup in all directions is less than 0.01.

Tertiary Electron Production

In the previous paragraphs it was shown that there is a nominal 0.18% error associated with the measurement of the proton current due to relativistic electrons emitted from the entrance foil. The measurement of

the current is further influenced by the tertiary electrons, the low-energy electrons resulting from electron-electron collisions in the copper cup and aluminum foil. To suppress the loss of tertiary electrons backscattered from the cup, a guard cylinder,[14] shown in Fig. 4, was installed, while a grid at the rear of the aluminum foil, also shown in Fig. 4, was used to minimize the fraction of tertiary electrons scattered from the foil to the cup.

Figure 5 shows the variation in the ratio of the ionization chamber current to the Faraday cup current as a function of the potential applied to the guard cylinder and grid of the cup. Over a change of 200 volts on the guard cylinder (zero volts on the grid) the ratio varies about 8%. For the same voltage change on the grid (zero volts on the guard cylinder) there is no measurable change in the ratio. These observations suggest the following explanation.

The secondary electrons produced in the copper by proton interactions generate low-energy tertiary electrons which escape into the re-entrant portion of the cup. With a positive potential upon the guard cylinder, these electrons are drawn out of the cup, thus increasing the apparent positive charge upon the cup above that due to the incident protons alone. Since the ionization chamber current remains effectively constant, the ratio of the ionization chamber current to the Faraday cup current becomes smaller. With a negative voltage on the guard cylinder, however, the tertiary electrons are turned back into the cup, the current measured is that due to the protons only, and the ratio of ion chamber current to Faraday cup current becomes larger. With a negative voltage upon the guard cylinder, a point is reached at which the ratio becomes constant, indicating that no measurable fraction of tertiary electrons is escaping. With a positive voltage on the cylinder the ratio continues to decrease as the potential is increased.

Schultz and Pomerantz,[15] studying secondary electron emission from a foil under bombardment by relativistic electrons, obtained results

---

14. B. Cork, L. Johnson, and C. Rickman, Phys. Rev. 79(1), 71 (1950).
15. A. A. Schultz and M. A. Pomerantz, Phys. Rev. 130, 2135 (1963).

similar to those of Fig. 5 when they measured the ratio of the current from their foil to that from a Faraday cup. They reported that the yield of low-energy electrons can be as high as 10%, depending upon the energy of the primary electron and the angle at which it strikes the foil. It is not unreasonable, therefore, to assume that for isotropic production of tertiary electrons in the copper cup, such electrons could cause the 8% variation shown in Fig. 5.

For the performance of the ionization chamber calculations it was assumed that a negative potential on the guard cylinder suitably prevented the escape of tertiary electrons from the cup. This assumption was reinforced by the observation that with a negative potential on the cylinder the value for the calibration of the ionization chamber more nearly approached the calculated value. It was also assumed that low-energy electrons from the entrance foil had negligible effect upon the calibrations. Since the results shown in Fig. 5 indicated that with negative potentials greater than -300 V the calibration was constant, the guard cylinder was operated at this potential.

Ion Formation in the Cup

To prevent ion formation in the residual gas surrounding the collection cup, the housing was evacuated with a diffusion pump connected to the vacuum port shown in Fig. 4. The pressure was measured by an ionization gauge mounted at the inlet to the pump to be $\sim 10^{-6}$ mm Hg. After correction for the length of the hose and the port diameter the nominal vacuum within the housing was 10^{-4} mm Hg. At this pressure the error due to ionization of the residual gas was of the order of 0.05%.

Connector Leakage

The loss of charge from the Faraday cup by connector leakage was reduced by using selected components having leakage resistances greater than 10^{14} Ω. This value was arrived at by measuring the leakage currents through the connector when 100 V was applied to the outer housing. The insulation of the Teflon mountings was assumed to be 10^{14} Ω or more, based upon the published values for its volume resistivity. During operation

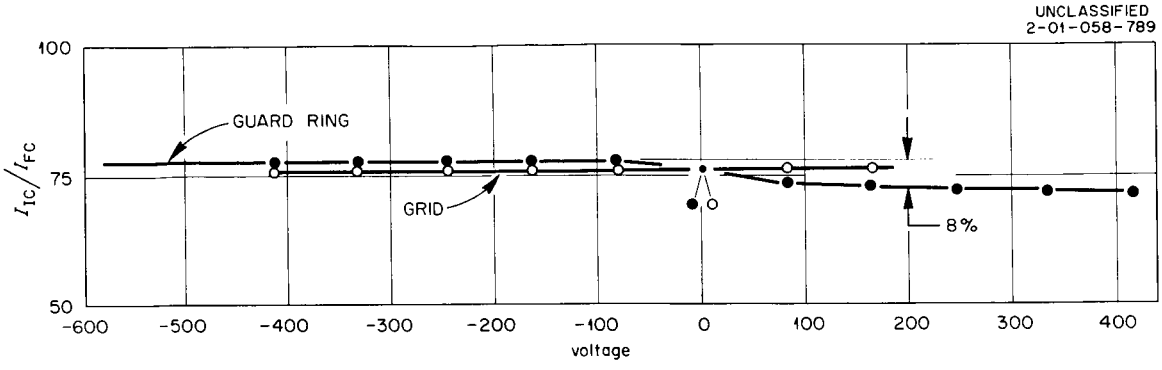

Fig. 5. The Effects of Variation of Guard Ring and Grid Voltage on the Apparent Calibration of the Ionization Chamber.

the voltage across the connectors was a few millivolts, so that the leakage was negligible when compared with measured currents of 10^{-14} A.

V. Electronics for Current Measurements

The charge collected by the Faraday cup was measured with a vibrating-reed electrometer,[16] of the type described by Fairstein.[17] The basic circuit of the instrument is shown in Fig. 6. The vibrating-reed electrometer was preferred over vacuum tube types because of its inherent capability of measuring low-magnitude currents. In a vacuum tube electrometer the signal and input tube variations are both amplified, thus the minimum input signal is limited by the grid current leakage of the electrometer tube. The vibrating-reed electrometer, on the other hand, is a null-seeking instrument in which the voltage drop due to the flow of current across the high resistance R_i of Fig. 6 is balanced out by the feedback voltage E_r. Any error in the balance produces a charge on the vibrating capacitor C_v. The resulting a-c signal is amplified through a preamplifier and the main amplifier. A fraction of the rectified signal, proportional to the error, is fed back to R_i, maintaining the junction P near zero potential. In addition to being able to measure currents smaller than the limiting grid leak currents of vacuum-tube models, the vibrating-reed electrometer has a drift rate 10 times smaller and a sensitivity nearly 100 times greater than vacuum tube electrometers.

For the smallest R_i used, 10^{10} Ω, and approximately 100 pF input capacitance, the pulsed nature of the proton beam produced negligible input voltage fluctuations.

The output signal of the electrometer was fed to an electronic integrator,[18] from which a count rate proportional to E_r was obtained. This instrument operates on a millivolt signal obtained by tapping the voltage across the meter of the electrometer. The input signal varies from 0 to 25 mV, corresponding to the zero to full-scale deflection of the meter.

16. Cary Model 31 Vibrating-Reed Electrometer, Applied Physics Corp., Monrovia, California.

17. E. Fairstein, Nuclear Instruments and Their Uses, Vol. I (ed. by A. H. Snell), Wiley, New York, 1962.

18. Royson "Lectrocount," Royson Engineering Co., Hatboro, Pennsylvania.

UNCLASSIFIED
ORNL-DWG 63-8259

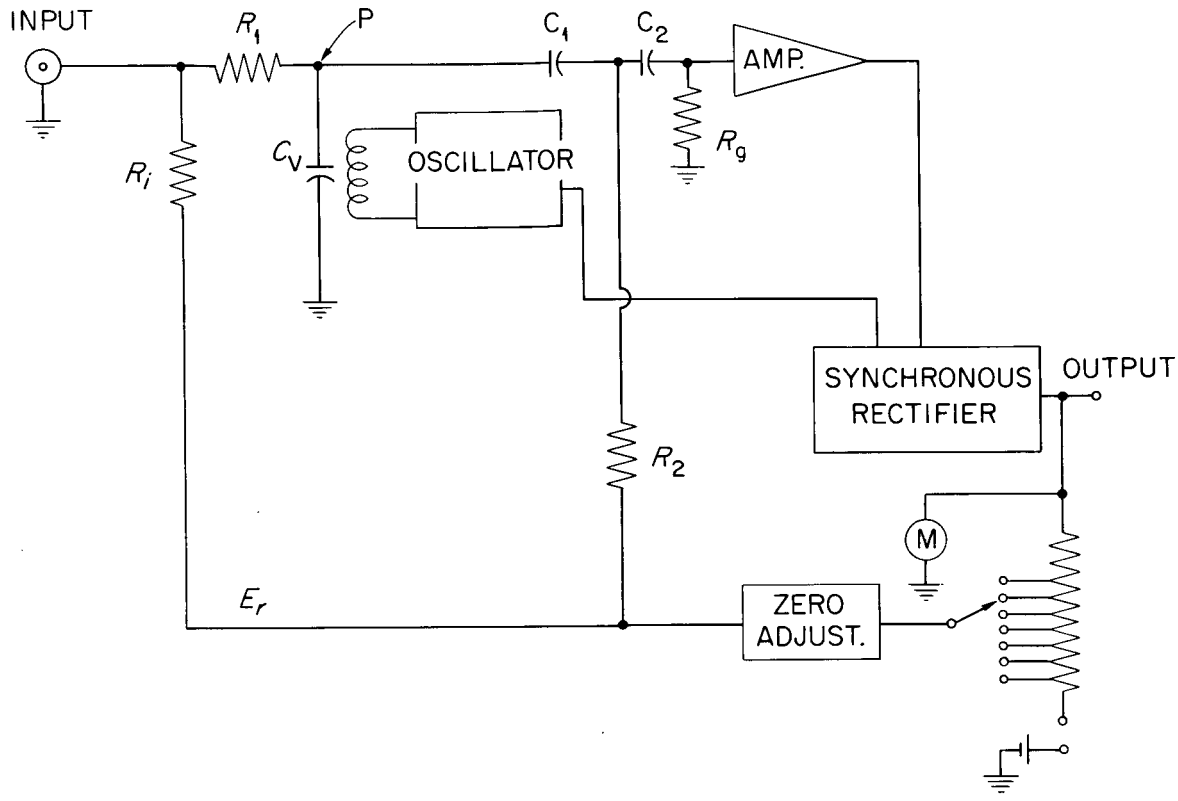

Fig. 6. Block Diagram of the Vibrating-Reed Electrometer Circuit.

The output rate is 1000 cpm at the full-scale value of E_r and, as shown in Fig. 7, varies linearly with input. The integrator is stable and has high speed of response.

The charge on the Faraday cup is obtained from the total number of integrator counts, using the relation

$$Q = (6 \times 10^{-2}) \frac{E_{SW}}{R_i} (\text{total counts}) , \qquad (7)$$

where E_{SW} is the value of the voltage set by the voltage selector switch on the electrometer panel. The errors associated with the measurement of Q will be discussed later.

The current from the ionization chamber was measured with an ORNL Q2525-2 current integrator.[19] This instrument, a diagram of which is shown in Fig. 8, integrates the input current and produces a pulse rate output proportional to the input current. The integrator operates in the following fashion.

A current from the ionization chamber charges capacitor C_1 so that

$$Q_1 = C_1 V_1 , \qquad (8)$$

where

Q_1 = charge, in coulombs,

C_1 = capacitance, in farads,

V_1 = voltage drop across C_1, in volts.

The electrometer circuit signal (amplified V_1) is fed to the pair of differential amplifiers, each having a gain of 250. The output of these amplifiers triggers a modified Schmitt trigger circuit when the voltage across C_1 reaches a specific value determined by the trigger set-point. The triggered signal is fed to a cathode follower through a pulse shaping circuit. Finally the pulse output is fed to a scaler through a cable driver network.

---

19. Designed by F. M. Glass, Instrumentation and Controls Division.

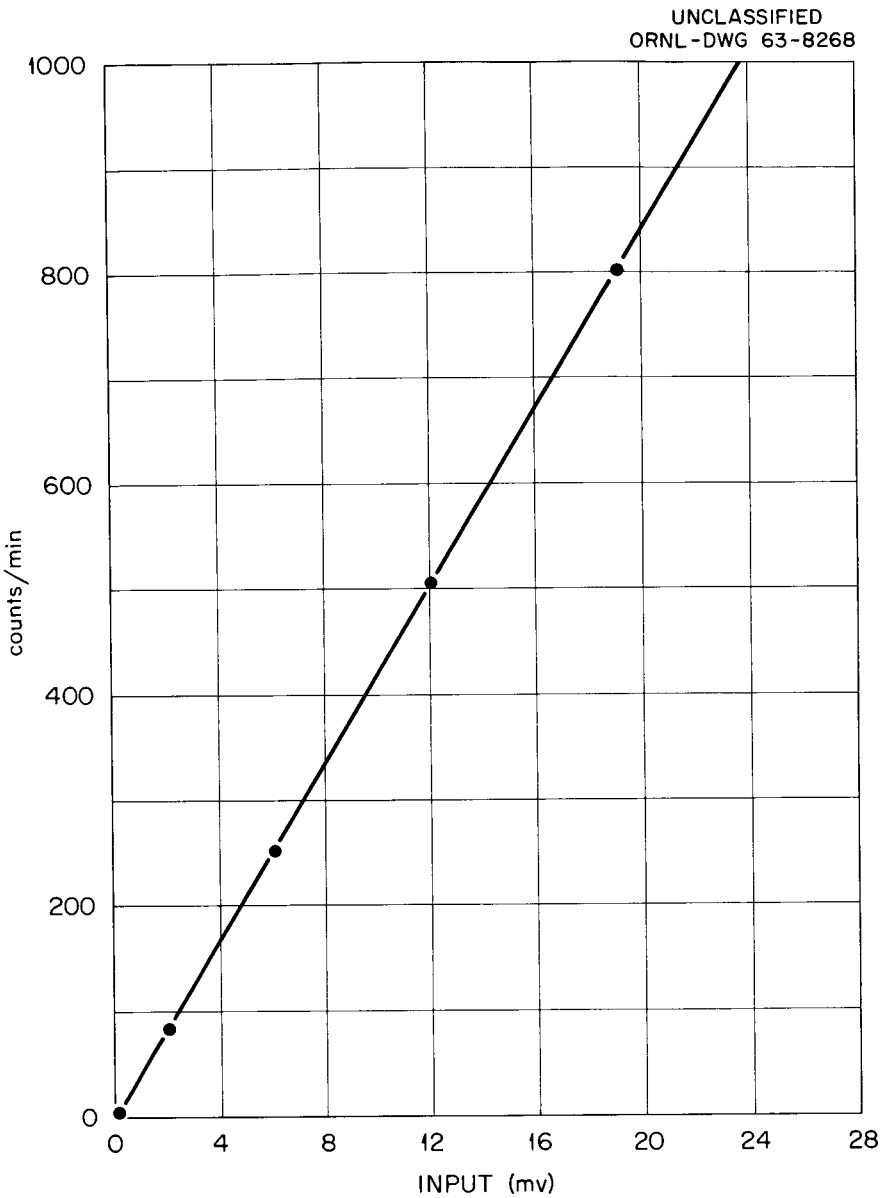

Fig. 7. Linearity Curve for the Royson "Lectro-count" Integrator.

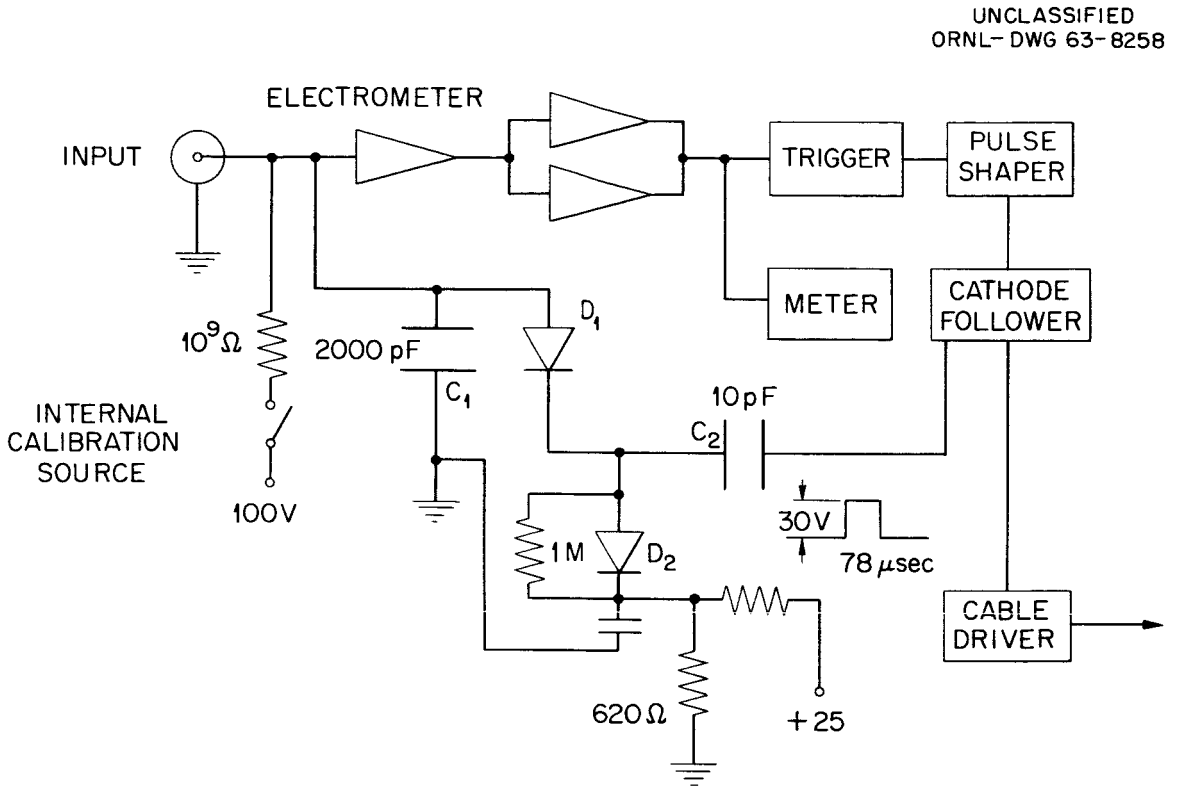

Fig. 8. Block Diagram of the Low-Range D-C Integrator Circuit.

The cathode follower generates a pulse of 30 V peak with a duration of 78 μsec. This pulse is impressed upon capacitor C_2 so that

$$dQ_2 = C_2\ dV_2 = 30\ C_2\ , \tag{9}$$

where

Q_2 = charge, in coulombs,

C_2 = capacitance of C_2, in farads.

The duration of the pulse is sufficiently long that C_2 is charged to 30 C_2 before diode D_1 conducts and C_1 is discharged. A feature of this circuit is that the pulse duration and amplitude are constants of the circuit. Therefore, neither a gain change in the differential amplifiers nor a drift in the electrometer can affect the character of the cathode follower pulse, and the integration rate thus remains constant. The constancy of the pulse will clear the accumulated charge on C_1 by a fixed amount defined by C_2. This is advantageous in that the change in charge across C_1 is the only measurement necessary. The capacitance introduced by the ionization chambers and cables does not affect dQ_1, since only dQ_2 determines the calibration. Since $dQ_1 = dQ_2$,

$$dQ_1 = \frac{C_2}{C_1}\ dV_2\ C_1\ , \tag{10}$$

where $C_2\ dV_2/C_1$ is the voltage swing on C_1. The value of C_2 can be varied to permit integration at rates of either 0.2 or 20.0 ncoulombs/output pulse.

The upper limit on the counting rate is established by the "duty cycle" of the instrument, defined by the 78-μsec pulse duration and the integration rate, which is determined by the input current. The maximum integration rate is nominally 10^4 pulses/sec. The lower limit, determined by the electrometer leakage and diodes D_1 and D_2, is about 1 count/hr for the 0.2×10^{-9} coulomb/output pulse value which was used for all measurements.

VI. Calibrations and Data Collection

Current-measuring instruments were calibrated against three standard sources. Two were supplied by Dr. A. M. Koehler of the Harvard staff. Source No. 1 consisted of a 125-V mercury cell in series with a 10^{12}-Ω resistor and had an output of 1.34 (±1%) x 10^{-10} A. Source No. 2 was a 1.25-V battery in series with a 10^{12}-Ω resistor and had an output of 1.42 (±3%) x 10^{-12} A. The calibration of these sources against a standard cell and precision resistance is described in the appendix. Source No. 3, consisting of a radioactive source mounted in fixed geometry within a saturated ionization chamber filled with air at atmospheric pressure, was built by R. J. Scroggs[20] and the senior author. Its output was determined to be 2.32 (±3%) x 10^{-13} A by comparison with Source No. 1. No attempt was made to evaluate the effect of barometric pressure on this value.

Calibration of the Vibrating-Reed Electrometer

The vibrating-reed electrometer was calibrated against all three standard sources to determine its consistency in measuring the charge due to a known current for each of three values of R_i, nominally 10^{10}, 10^{11}, and 10^{12} Ω. The results are shown in Table 1. The standard source was connected to the electrometer input (see Fig. 6) and the apparent charge measured with the integrator. Since the current from the source was known, for a given value of electrometer full-scale voltage, E_{SW}, the charge due to the source current is determined. For any value of R_i the charge collected for a fixed time should be a constant and independent of the value of R_i. From Table 1 it is seen that only with the 10^{10}-Ω resistor does the measured current agree with the true current. The same errors in the resistor worths were observed when the currents from the sources were measured using a fixed value of R_i, with E_{SW} varied. The measurements of current made using the 10^{11}- and 10^{12}-Ω resistors must therefore be corrected by the factors shown in Table 1.

---

20. Instrumentation and Controls Division.

Table 1. Results of Current-Source Calibrations of Vibrating-Reed Electrometer Resistances

E_{SW}, Electrometer Full-Scale Voltage (V)	Input (Source) Current (A)	Nominal R_i (ohms)	Integrator Counts/min	Measured[a] Current (A)	Measured[b] R_i (ohms)	Correction Factor
3.00	$1.34(\pm 1\%) \times 10^{-10}$	10^{10}	450	1.35×10^{-10}	9.93×10^{9}	$1.01(\pm 1\%)$
30.00		10^{11}	598	1.79×10^{-10}	7.52×10^{10}	$1.33(\pm 1\%)$
0.030	$1.42(\pm 3\%) \times 10^{-12}$	10^{10}	476	1.428×10^{-12}	9.95×10^{9}	$1.01(\pm 3\%)$
0.300		10^{11}	631	1.89×10^{-12}	7.52×10^{10}	$1.33(\pm 3\%)$
3.00		10^{12}	551	1.65×10^{-12}	8.6×10^{11}	$1.16(\pm 3\%)$
0.010	$2.32(\pm 3\%) \times 10^{-13}$	10^{10}	77.3	2.32×10^{-13}	10^{10}	$1.00(\pm 3\%)$
0.100		10^{11}	104.6	3.14×10^{-13}	7.39×10^{10}	$1.35(\pm 3\%)$
1.00		10^{12}	90.3	2.71×10^{-13}	8.56×10^{11}	$1.17(\pm 3\%)$
0.030	$1.42(\pm 3\%) \times 10^{-12}$	10^{10}	473	1.42×10^{-12}	10^{10}	$1.00(\pm 3\%)$
0.300		10^{11}	674	2.03×10^{-12}	7.0×10^{10}	$1.43(\pm 3\%)$
3.00		10^{12}	533	1.63×10^{-12}	8.7×10^{11}	$1.13(\pm 3\%)$

a. The measured current is calculated from Eq. 12 by dividing the measured charge, Q, in coulombs by the time in seconds to collect the integrator counts.

b. R_i (meas) = R_i (nominal) x source current/measured current.

c. The true value of the current is obtained by dividing the measured current by the correction value. The mean value for the correction factor is: for 10^{10} ohms, 1.004 ($\pm 2.3\%$); for 10^{11} ohms, 1.358 ($\pm 2.3\%$); and for 10^{12} ohms, 1.165 ($\pm 3\%$).

Calibration of the Low Range D-C Integrator

So that both current-measuring instruments would be calibrated against the identical current standard, the low-range d-c integrator was calibrated using Source No. 1 as the input current source. The integration rate was adjusted to give 0.200×10^{-9} coulomb/count.

This method was adopted when it was observed that calibration against the internal source gave integration rates 4 to 9% higher than those obtained with Source No. 1. The internal current source consisted of 100 V in series with five 200 ($\pm$1%) Meg resistors. The voltage was checked with a precision voltmeter and found accurate to $\pm$0.25%. The differences between the integration rate obtained by using the internal source and that obtained with Source No. 1 were attributed to the resistor string of the internal supply.

After calibrating the integrator against the known source, the corresponding calibration against the internal source was obtained to use as a check for drift. Subsequent checks with both the internal source and with external sources showed the instrument was stable over the duration of the calibration experiments. Over extended periods (7 days) the calibration drift was less than 2%. Typical calibration data are shown in Table 2.

Data Collection

The general arrangement at the Harvard University Synchrocyclotron for energy spectrum measurements has been described elsewhere.[21] A block diagram of the arrangement for the calibration of the ionization chambers versus the Faraday cup is shown in Fig. 9. In this configuration the following measurements were made.

Ion Pairs/Proton vs. Beam Intensity. The number of ion pairs produced in the helium-filled chambers per proton was obtained from the ratio of the charge in the ionization chamber to that collected by the Faraday cup. The charge in the ionization chamber is

---

21. R. T. Santoro et al., Neutron Phys. Div. Ann. Progr. Rept., Sept. 1, 1962, ORNL-3360, p 272.

Table 2. Results of Calibration of the Low Range D-C Integrator Against Standard Current Source No. 1[a]

Integrator No.	Integrator Counts	Count Time (sec)	Integration Rate (coulombs/count)
			(x 10^{-9})
		Run No. 1	
2	100	155.1	0.212
2	100	155.2	0.207
2	100	155.1	0.212
2	100	155.4	0.208
1	20	31.7	0.218
1	20	31.7	0.218
1	20	31.7	0.218
1	20	31.7	0.218
2	20	31.1	0.213
2	20	31.0	0.213
		Run No. 2	
1	500	1.123	0.200
1	500	1.122	0.200
1	500	1.122	0.200
2	500	0.85	0.200
2	500	0.85	0.200
2	500	0.85	0.200
		Run No. 3	
1	10	15.17	0.200
1	10	15.17	0.200
1	10	15.17	0.200
1	10	15.17	0.200
2	10	15.21	0.200
2	10	15.21	0.200
2	10	15.21	0.200
2	10	15.21	0.200
		Run No. 4	
1	497	10	0.200
1	497	10	0.200
1	497	10	0.200
2	497	10	0.200
2	497	10	0.200
2	497	10	0.200

a. Source No. 1 = 1.34(±1%) x 10^{-10} A.

b. For Run No. 1 the instrument was calibrated against its internal source to give 0.2 x 10^{-9} coulomb/count. The integration rate tabulated is that obtained with Source No. 1 as the input current. For the other three runs the instrument was adjusted to give 0.2 x 10^{-9} coulomb/count from Source No. 1. The run numbers refer to the energy-spectral runs referred to in the text.

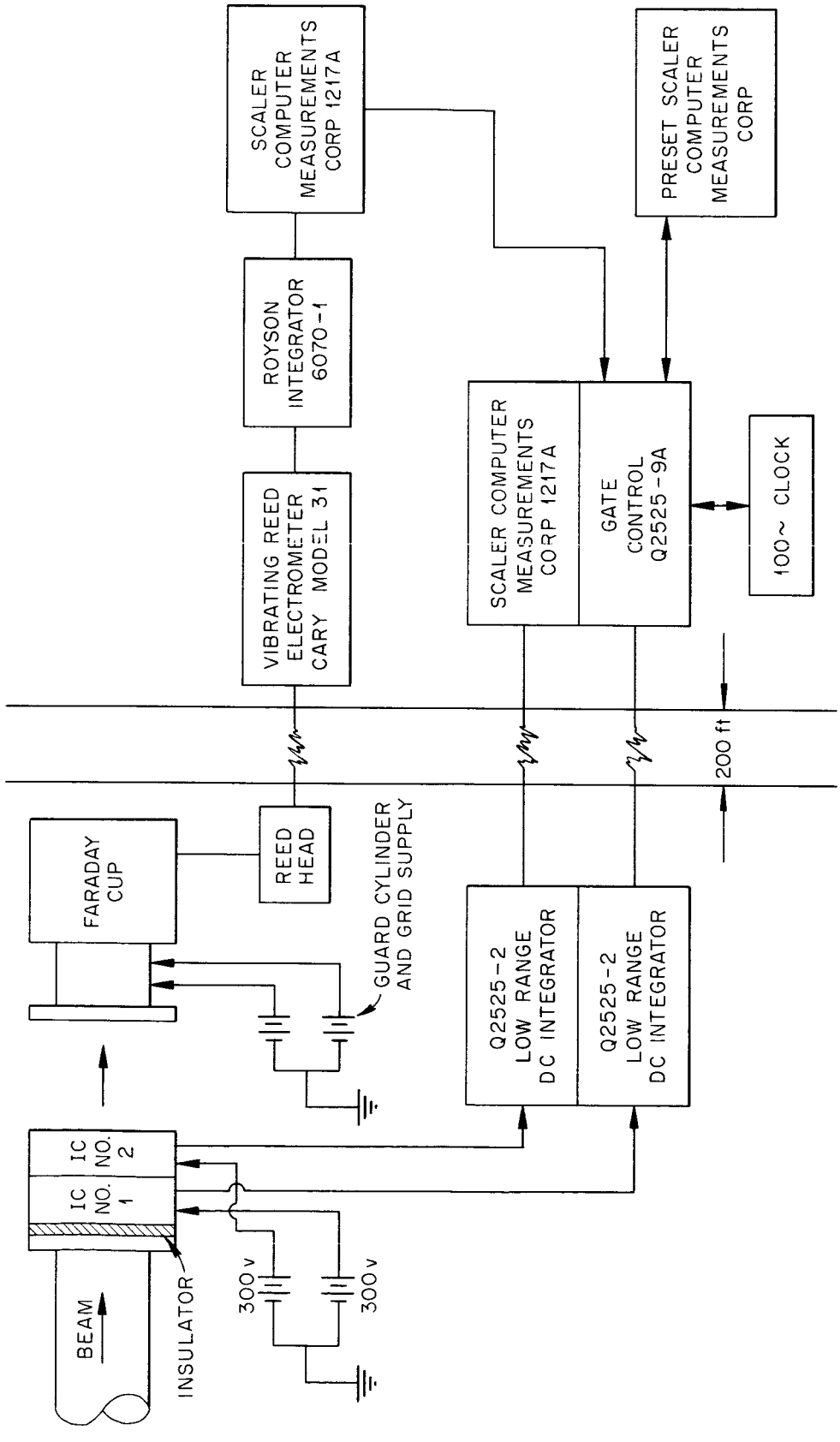

Fig. 9. Block Diagram of the Ionization Chamber Calibration Circuit.

$$Q_{ic} = 1.602 \times 10^{-19} \text{ (Pt)(ip/proton)}, \tag{11}$$

and the charge in the Faraday cup is

$$Q_{FC} = 1.602 \times 10^{-19} \text{ (Pt)} , \tag{12}$$

where

P = beam intensity, in protons/sec,

t = duration of measurement, in sec.

For a common time, t, the number of protons passing through the ionization chamber is obviously equal to the number entering the cup. Then

$$Q_{IC}/Q_{FC} = \text{ion pairs/proton} = IP. \tag{13}$$

From this ratio, the quantity IP was experimentally determined for several beam intensities.

Proton Beam Intensity. The beam intensity, IP, having been determined, is calculated by rearranging the terms of Eq. 12:

$$P = \frac{6.242 \times 10^{18} \, Q_{IC}}{IPT} . \tag{12a}$$

Number of Protons per Integrator Count. The collection of data in the energy-spectral experiments was controlled by the number of integrator counts necessary for obtaining acceptable secondary-particle spectra statistics. The number of protons per integrator count is obtained from Eq. 12:

$$\frac{Pt}{\text{counts}} = \frac{1.248 \times 10^{9}}{IP} , \tag{12b}$$

since

$$Q_{IC} = \text{counts} \cdot 0.2 \times 10^{-9} \text{ coulomb/count}.$$

Preliminary data were taken at several beam intensities to determine the number of integrator counts recorded as a function of time. The Royson Lectrocount could be adjusted to give nominally 500 counts/min or more by setting E_{SW} to produce mid-scale deflection of the meter. The low-range d-c integrator count rate, however, depended on the magnitude of the input current from the ionization chamber. At beam currents of about 8×10^{-5} A the integrator recorded 1 count/45 sec. This rate corresponds to $\sim 5 \times 10^{4}$ protons/sec, which is within the range of the measurements desired. At beam currents of 10^{-11} A, the integrator recorded 16 counts/sec.

The calibration data were obtained for a fixed number of integrator counts, controlled by the preset scaler. The gating circuit shown in Fig. 9 opened after recording one count from the integrator and remained open for the number of counts preset in the scaler. Regardless of the fraction of charge originally in the ionization chamber, the data were obtained for an integral number of integrator counts.

The integrator counts from the second ionization chamber were recorded by a gated scaler. The data could contain an error of ± 1 count depending upon the fraction of charge in the chamber when the gate opened. To account for this fraction, the deflection of the panel meter, which goes from zero to full scale for each count, was noted at the opening and closing of the gate. The number of counts recorded plus the fraction of deflection at the start and at the end of each run gave the true value of counts, or the true charge. At high counting rates the fractions of charge were treated as a small error contribution.

The counting error in the data from the vibrating-reed electrometer was negligible, since for all measurements E_{SW} was set for a count rate greater than 500 counts/min. The error due to the fraction of charge initially in the Faraday cup was therefore less than 0.2%. The only significant error in the measurement of the charge collected by the cup was the 3% contributed by the uncertainty in the calibration of the electrometer resistances.

The error in the measurement of the charge collected by the ionization chamber consisted of the 1% uncertainty in the calibration of the

low-range integrator and the ±1 count uncertainty in the integrator counts, which was significant only at low count rates.

VII. Results of Calibration Runs

The results of four calibrations of the ionization chambers against the Faraday cup are shown in Figs. 10-12 and 15. Each calibration was made just prior to a particular set of energy-spectral measurements and is conveniently identified by association with that set.

Run No. 1

The data of Run No. 1 were used for a series of experiments testing the feasibility of Bonner spheres and threshold detectors for neutron spectroscopy at energies from 10^{-7} to 10^{2} MeV (Ref. 22) and for the dosimetric experiments of Maienschein and Blosser.[23] These data are plotted in Fig. 10. The beam intensity during this run ranged from 10^{7} to 10^{10} protons/sec. The results show a difference between the responses of the two ionization chambers of 5.7%. This difference stems from variations in the construction of the two chambers. Tests made with a Sr^{90} source in fixed geometry relative to the ionization chambers also showed that the ratio of chamber currents, I_{IC-1}/I_{IC-2}, was 1.06.

Run No. 2

The information from Run No. 2 was used in connection with the measurements of the gamma-ray spectra from proton-bombarded nuclei, reported by Zobel et al.[24] In this calibration the response of the ionization chambers was measured over a range of beam intensities from nominally 2×10^{6} to 2×10^{9} protons/sec. The data are plotted in Fig. 11. The agreement with the data of Run No. 1 is very good and, considering that

---

22. W. R. Burrus, Neutron Phys. Div. Ann. Progr. Rept., Sept. 1, 1962, ORNL-3360, p 296.

23. F. C. Maienschein and T. V. Blosser, The Depth-Dose Distribution Produced in a Spherical, Water-Filled Phantom by the Interactions of a 160-MeV Proton Beam, ORNL-3457 (June, 1963).

24. W. Zobel, F. C. Maienschein, and R. J. Scroggs, Neutron Phys. Div. Ann. Progr. Rept., Aug. 1, 1963, ORNL-3499 (Vol. II), p 66.

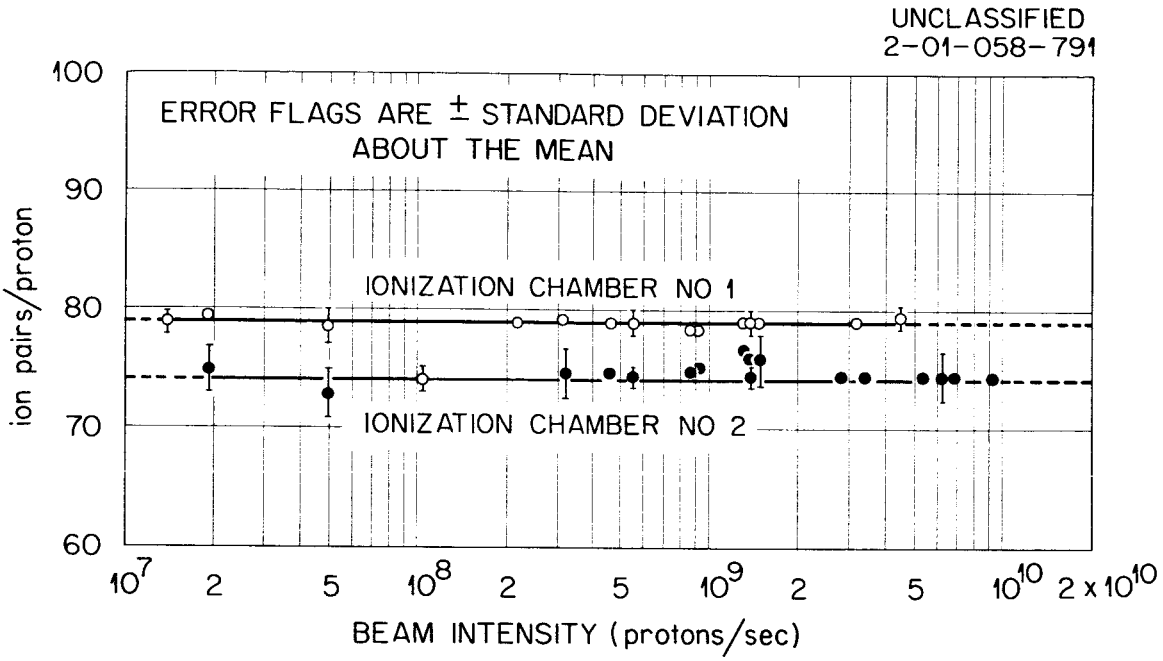

Fig. 10. Ionization Chamber Calibration Curves: Run No. 1.

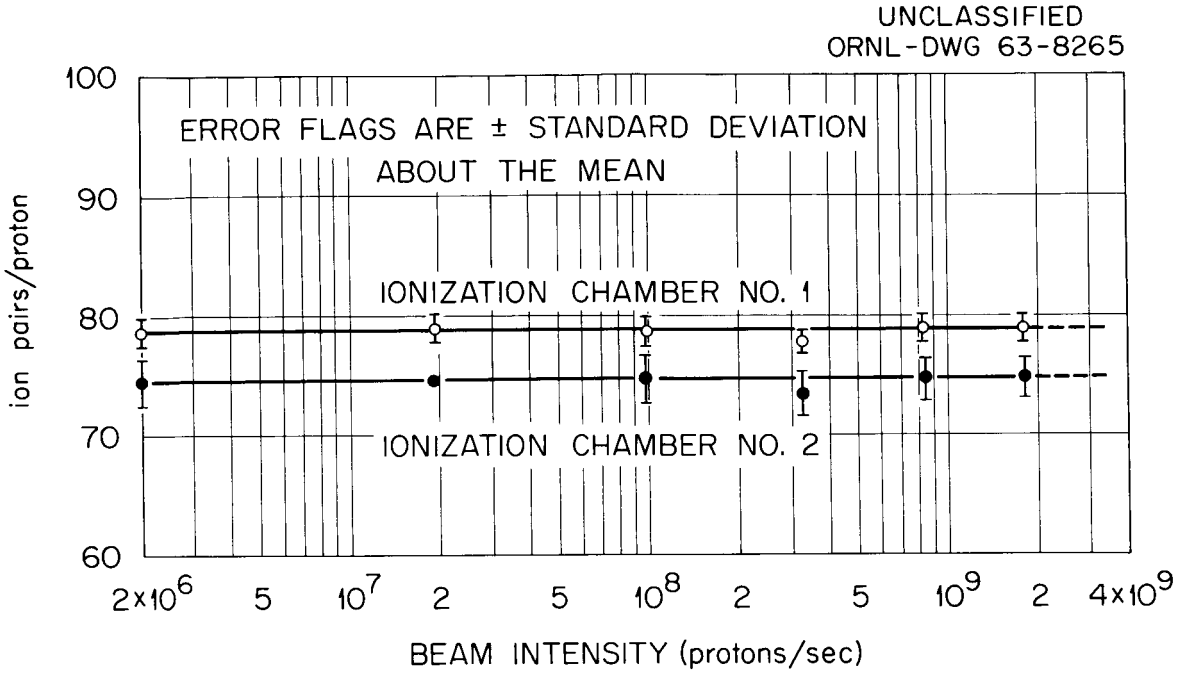

Fig. 11. Ionization Chamber Calibration Curves: Run No. 2.

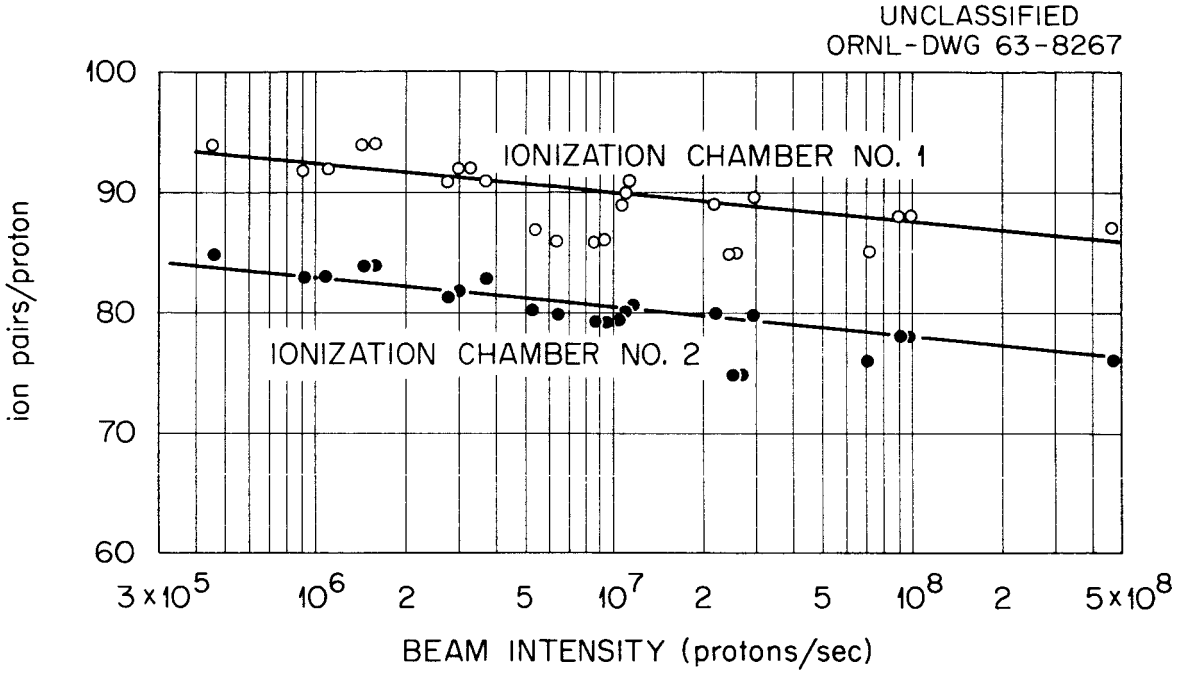

Fig. 12. Ionization Chamber Calibration Curves: Run No. 3.

the runs were separated by several weeks, indicates that the measurement techniques were reliable and that leakage of gas from the chambers was negligible.

Run No. 3

The calibrations of Run No. 3 were made for the measurements of neutron and proton spectra with proton recoil telescopes reported by Wachter et al.[25] The ionization chamber response was measured over a range of 5×10^5 to 5×10^8 protons/sec.

The results of the calibration are shown in Fig. 12. In contrast to the results of Runs 1 and 2 shown in Figs. 10 and 11, the response curve for Run 3 is not flat, but slopes downward at a rate of 2.9%/decade, or 2.5 ip/proton per decade of beam intensity.

Analysis of the data of Fig. 12 suggests that the slope results from systematic errors in the instrumentation. The slope of the response curve for each chamber is the same, and, as Fig. 13 shows, the ratio of the charge collected in ionization chamber No. 1 to that collected in ionization chamber No. 2 is constant ($\sim$ 1.10) over the range of beam intensities for which the calibration was made. This ratio is in agreement with the ratio of the measured values of Fig. 12.

Figure 14 shows the ratio of the counts obtained from the vibrating-reed electrometer integrator (the Royson Lectrocount) to those obtained from the low-range d-c integrator with each connected to an ionization chamber. The ratio is plotted as a function of electrometer full-scale voltage, E_{SW}. The slope of the curve is 2.3%, which corresponds reasonably well to the slope of the calibration curve of Fig. 12. This suggests that the non-flat character of the calibration curve is due to nonlinearities in the voltage scales.

Measurements of the ionization chamber responses taken during a period preceding calibration Run 3 gave a value of 84.3 $\pm$ 1.7 ip/proton for 17 observations with chamber No. 1, and a value of 77.1 $\pm$ 3.8 ip/proton

---

25. J. W. Wachter et al., Neutron Phys. Div. Ann. Progr. Rept., Aug. 1, 1963, ORNL-3499 (Vol. II, p 89.

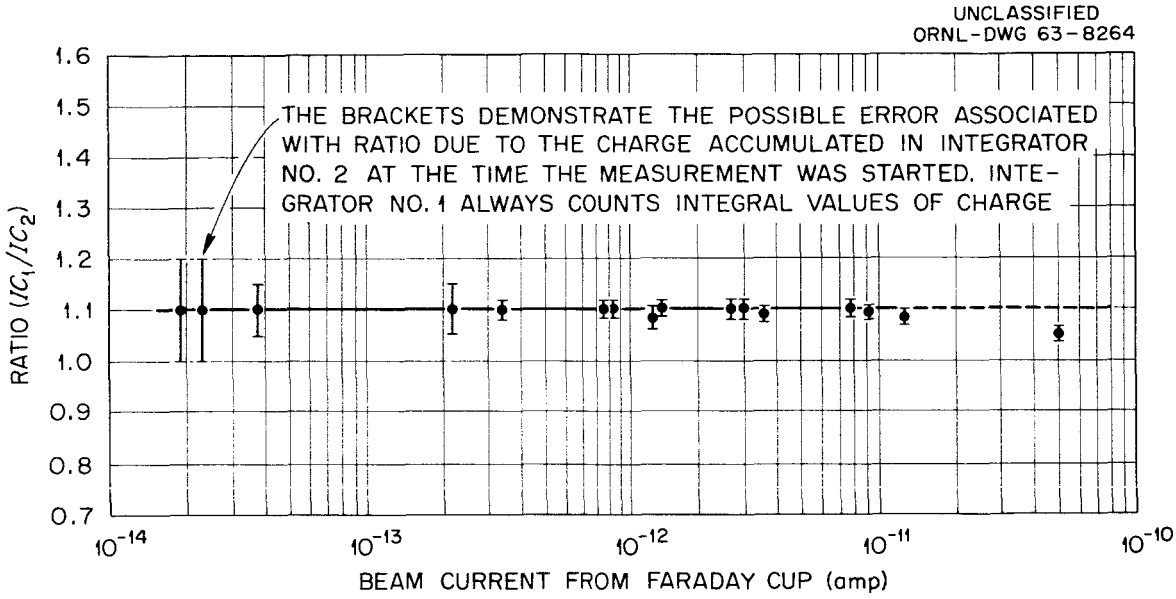

Fig. 13. Ratio of the Charge Measured in Ionization Chamber No. 1 to That Measured in Chamber No. 2 as a Function of the Beam Current Measured with the Faraday Cup.

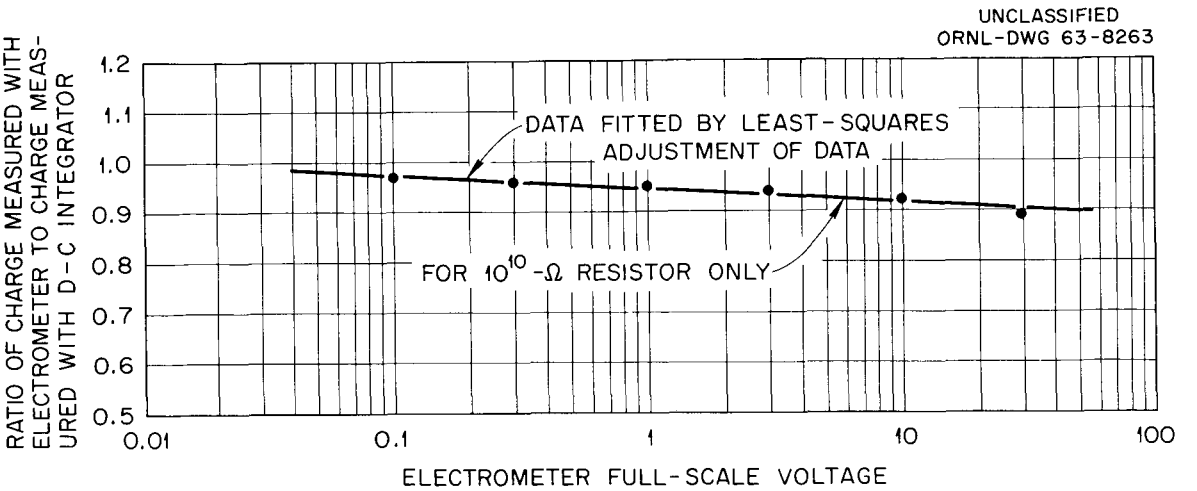

Fig. 14. Ratio of the Responses of the Vibrating-Reed Electrometer and the D-C Integrator to an Equal Charge Collected in an Ionization Chamber as a Function of Electrometer Full-Scale Voltage.

for 16 observations with chamber No. 2. The range of beam intensities was from 10^5 to 10^8 protons/sec. These values are 7.5% and 4.0% higher, respectively, than the values obtained for chambers 1 and 2 during the first two calibration runs.

System failure occurred just previous to Run No. 4. Investigation showed a defective electron tube in the Royson Lectrocount. Examination of the influence of the failure suggests that the output signal of the vibrating-reed electrometer may have been affected by feedback of a d-c voltage from the Lectrocount to the electrometer. Although this explanation seems plausible, it was not proved. However, replacing the tube for Run No. 4 eliminated the nonlinearities.

The calibration data for Run No. 3, Fig. 12, were corrected by 2.5% per decade of beam intensity, taking the value of response measured with E_{SW} as the true value.

Run No. 4

Calibration Run No. 4 was made in support of the flight-time spectral measurements of secondary neutrons and protons from reactions of 160-MeV protons with various nuclei, reported by Peelle et al.[26] The calibration data, obtained over a range of beam intensities from 4×10^4 to 3×10^9 protons/sec, are plotted in Fig. 15.

Summary of Calibrations

The data of the four calibration runs are summarized in Table 3. Comparison of the results of Run No. 4 with those of Run No. 1 shows that the value for ip/proton increased by 6.7% for ionization chamber No. 1 and by 5.5% for ionization chamber no. 2 over the four-month period separating the first and last runs. This change in response with time was verified by comparison of measurements with a Sr^{90} source made just previous to Runs 1 and 4, which showed the same increase. The change was probably due to contamination of the helium in the chambers increasing as a function

---

26. R. W. Peelle et al., Neutron Phys. Div. Ann. Progr. Rept., Aug. 1, 1963, ORNL-3499 (Vol. II), p 73.

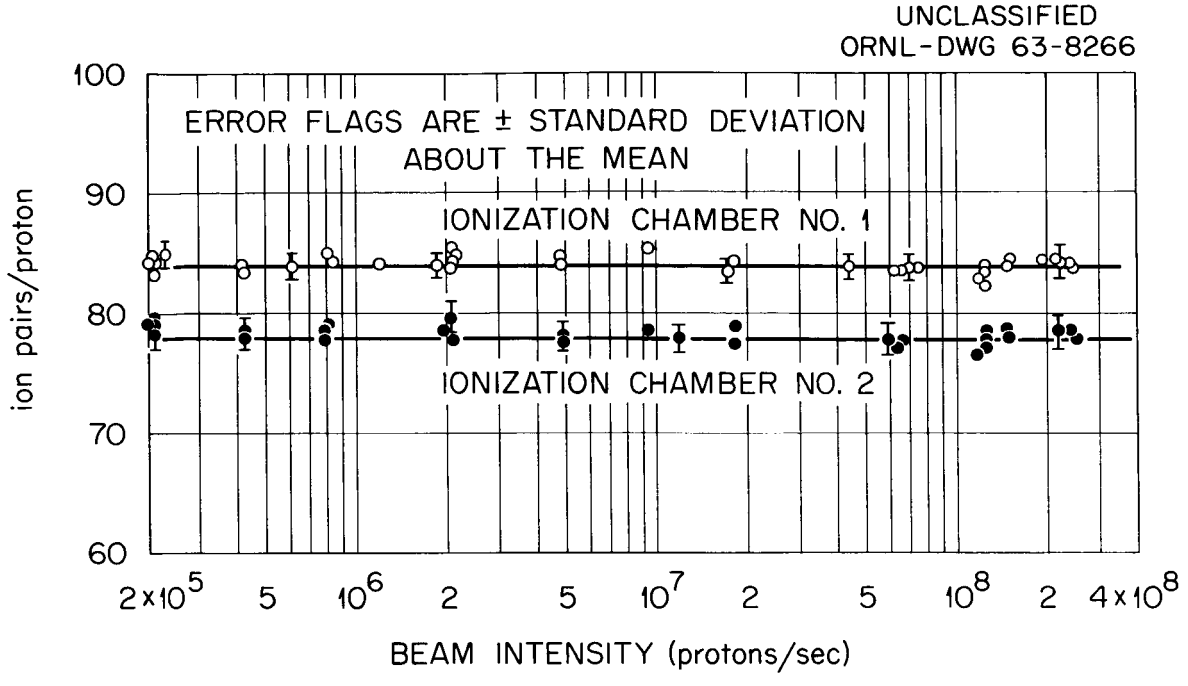

Fig. 15. Ionization Chamber Calibration Curves: Run No. 4.

Table 3. Ionization Chamber Parameters for Four Runs

	Ionization Chamber No. 1				Ionization Chamber No. 2			
	Run 1	Run 2	Run 3	Run 4	Run 1	Run 2	Run 3	Run 4
Number of Observations	21	9	27	38	21	9	27	38
Average Ion Pairs/Proton	79.04	78.37	85.47[a]	84.36	74.75	74.11	77.05[a]	78.94
Std. Dev of the Mean	0.310	0.532	1.20	1.38	1.09	1.10	1.35	1.72
Frac Std Dev of Mean	0.0039	0.0068	0.014	0.016	0.0145	0.0148	0.0175	0.021
Std. Dev of the Data	1.386	1.504	7.27	8.20	4.87	3.11	9.09	10.4
Frac Std Dev of Data	0.0175	0.0192	0.085	0.098	0.0652	0.0420	0.117	0.132
Faraday Cup Error from Electron Collection (Ion Pairs/Proton)	-0.14	-0.14	-0.15	-0.15	-0.13	-0.13	-0.14	-0.14
Best Value for Ion Pairs/Proton	78.9 ± 0.39%	78.2 ± 0.68%	85.3 ± 1.4%	84.2 ± 1.6%	74.6 ± 1.5%	74.0 ± 1.5%	76.9 ± 1.8%	78.8 ± 2.1%
Percent Error (IP_{meas}/IP_{calc}) (IP_{calc} = 80.4 ± 3.5%)	-1.9%	-2.7%	+6.1%	+4.7%	-7.3%	-8.0%	-4.4%	-2.0%
Average Calibration of Ion Chamber Current Integrator (Coulomb/Count)	0.218(±1%) x 10^{-9}	0.200(±1%) x 10^{-9}	0.200(±1%) x 10^{-9}	0.200(±1%) x 10^{-9}	0.213(±1%) x 10^{-9}	0.200(±1%) x 10^{-9}	0.200(±1%) x 10^{-9}	0.200(±1%) x 10^{-9}
Protons per Integrator Count	1.72(±0.39%) x 10^{-7}	1.60(±0.68%) x 10^{-7}	1.46(±1.4%) x 10^{-7}	1.48(±1.6%) x 10^{-7}	1.78(±1.5%) x 10^{-7}	1.69(±1.5%) x 10^{-7}	1.62(±1.8%) x 10^{-7}	1.58(±2.1%) x 10^{-7}

a. Best average value from corrected data.

of time. The value of W for pure helium is 42 ev/ion pair. The admixture of as little as 2% air will reduce this value to about 29 ev/ion pair, the value used in the calculation of the ionization chamber response (Eq. 2), which assumed helium of 98% purity.

VIII. Ionization Chamber Calibration by Direct Proton Counting Techniques

Introduction

Since perfect performance of a Faraday cup is not assured *per se*, and since fast counting equipment was available, an independent calibration of the ionization chambers was performed by directly counting the protons responsible for the collection of a measured charge in either ionization chamber.

Preliminary comparisons of this type were obtained during feasibility trials at Harvard in 1962, but the results were not reproducible because of incomplete fast scaling equipment.

In order to count the protons in a beam, it is essential that the proton current be reduced to a level at which counting losses are not beyond correction. Synchrocyclotron beams are divided into microstructure bursts having the rf acceleration frequency and a width of a few nsec, generally less than one counting resolution. Therefore only one pulse can be counted per rf period. If the counting equipment can respond once per rf period (42 nsec at Harvard), the only "losses" arise because the scaler is unable to detect whether only one proton is present in a microstructure burst or more than one. If m is the mean number of protons per burst in a steady beam, and its value is small, the fraction of protons which occur in such multiple-proton bursts is about m/2. In our case m was kept between 0.05 and 0.1 (0.08, typically), and a correction was applied for the $\sim$ 4% loss. Since the quadratic macroburst duty factor at the Harvard Synchrocyclotron during our experiment was about 0.025, proton count rates were limited by counting problems to the region below 5×10^4 protons/sec.

During the run using the flight-time spectrometer, readings of charge collected by either ion chamber were recorded for each experimental

run, along with sums of scaler counts obtained from three circuits associated with a pair of thin scintillators placed in the proton beam. The range of beam currents represented by the data is very small, and the level of attention paid the ion chamber and electrometer during the data runs was minimal, but a body of data resulted in which the count of protons in the beam can be given high credibility.

Apparatus

Figure 16 shows the geometry of the important parts of the equipment. The helium-filled ionization chambers were attached to the end of the beam tube some 46 cm in air from the pair of scintillators.

The scintillation detector consisted of two parallel 1-mm-thick plastic scintillators, each effectively about 1.5 in. in diameter, mounted about 18 cm apart and with the beam striking the center of each detector within a fraction of a centimeter. Each scintillator was covered with about 0.001 in. of aluminum on each surface. The 1-mm-thick counters absorbed about 0.5 MeV from each penetrating proton. Figure 17 shows a pulse-height spectrum (charge pulses) obtained at a low count rate, using a coincidence trigger arrangement to avoid detection of noise pulses.

Each scintillator was attached to a Phillips 56 AVP multiplier phototube. In each case the signal from the 14th dynode was fed into a long 125-Ω coaxial cable resistively terminated at the input end and approximately terminated by a differentiating pulse transformer at the output end. A timing signal was obtained from each pulse by means of a Bergman-type[27] tunnel diode univibrator, and these two timing signals were mixed in a similar univibrator which acted as a coincidence circuit with a resolving time of about 4 nsec, adequate to cover the apparent timing jitter. Thus coincident events were counted with high efficiency, while noise from detection of miscellaneous radioactivity could produce a count only with great difficulty.[28]

---

27. R. H. Bergman, M. Cooperman, and H. Ur, RCA Rev. 23, 152 (1962).
28. The coincidence circuit and other electronic components were designed by N. W. Hill and R. J. Scroggs of the ORNL Instrumentation and Controls Division.

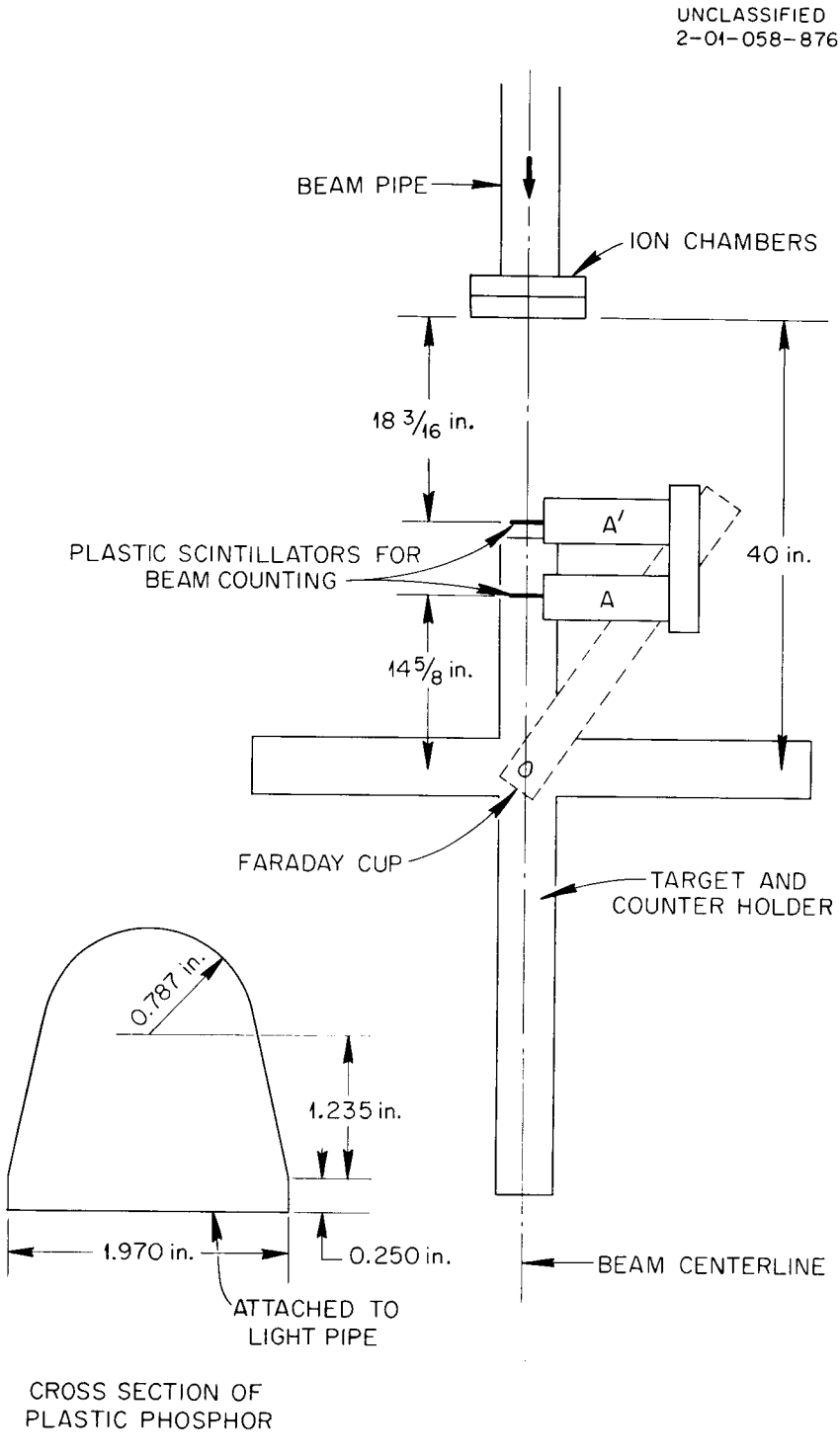

Fig. 16. Experimental Arrangement for Ionization Chamber Calibration by Direct Counting of Beam Protons.

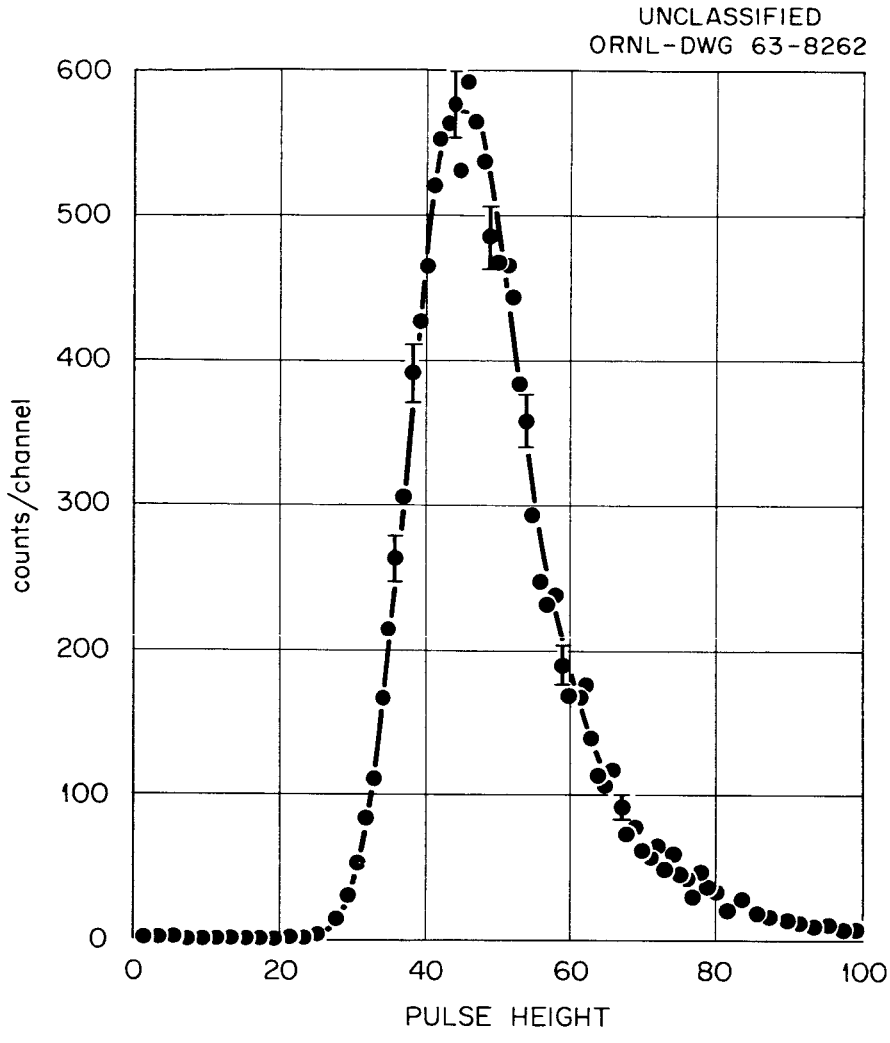

Fig. 17. Pulse-Height Spectrum Resulting from Passage of 160-MeV Protons Through the 1-mm-thick A' Detector.

The output from this coincidence circuit could be scaled either by a modified 10-Mc Computer Measurements Corporation scaler with a driver having a 30-nsec pulse-pair resolution, or by a pair of 100-Mc Eldorado model 1040 fast prescalers. When tested, the driver for the prescalers, fed by the coincidence circuit, performed well with pulse trains of four pulses spaced 10 nsec apart. These prescalers were somewhat temperamental, leading to the uncertainties discussed below. The main point is that with either scaler system one could expect to count two protons if they occurred in successive proton microstructure bursts, while with the fast prescaler system one could expect occasional detection of two protons within the same microburst. Oscilloscope observations, however, did not indicate any detections of the latter type.

The pulses from the coincidence counters were handled by additional logic circuits to be described in a later report on the flight-time spectroscopy. In addition to the coincidence counts, two other counts were obtained from each run. One of these was the number of proton-containing microbursts which were both preceded and followed by two microbursts that did not contain protons. The second consisted of the counts registered in an entirely separate coincidence circuit designed to detect most of the microbursts in which more than one proton passed through the scintillators.

A comparison of either of these counts with that from the fast scaler gives enough information to estimate the synchrocyclotron quadratic duty factor and thence the actual number of protons penetrating the two counters.

Analysis of the Counting Data

The validity of the comparison proposed depends on the premise that each proton which produces charge in the ionization chamber also passes through the scintillators and produces a count from the fast coincidence circuit, unless another proton in the same microburst has already produced such a count. Four types of difficulties challenge the validity of this assumption and are dealt with in this section. As an initial difficulty,

the fast coincidence circuit may have less than unit efficiency because of time jitter between its input signals too large for the resolving time employed.

To study this question one examines data showing the relative count rate in the AA' coincidence circuit as a function of signal delays introduced into one of the cables connecting the circuit to a detector. Figure 18 shows typical data. Such curves can be analyzed to estimate values of the coincidence efficiency by assuming an underlying normally distributed timing jitter to be responsible for the non-perpendicular slopes on the sides of the delay curve. It is believed that this method is only weakly dependent on the exact form of the jitter distribution. Analysis of the 10 checks obtained during the course of the experiment indicates coincidence efficiencies between 99.8% and 99.1%. A coincidence efficiency of 99.5 ($\pm$0.5%) was assumed for the analysis of the ionization chamber calibration data.

A second difficulty stems from uncertainties in the determination of the best value of Q, the number of protons passing through the detector system during a run, based on scaler readings. The auxiliary scaler data noted earlier were analyzed to give the quadratic duty factor, f, consistent with observed counts. The analysis was performed[29] by solving the non-linear equations which result when the expected count of each scaler is expressed in terms of Q and of the macroburst structure of the beam. A Newton iterative method for two or six equations was employed. Since there were as many parameters as input data, "sense" could be made of the solutions obtained only in terms of the reasonableness of the parameters and the constancy thereof. Three or four models were used to relate the scaler readings to the unknowns and, since the resulting values of Q are not model-dependent by more than 0.3%, the uncertainty produced by duty cycle effects in the estimate of total protons in a run was estimated to be 0.3%. However, the full uncertainty in the value of Q is principally dependent on the accuracy of the fast scaler readings discussed below.

---

29. The analysis and many other calculations were performed by R. L. Cowperthwaite.

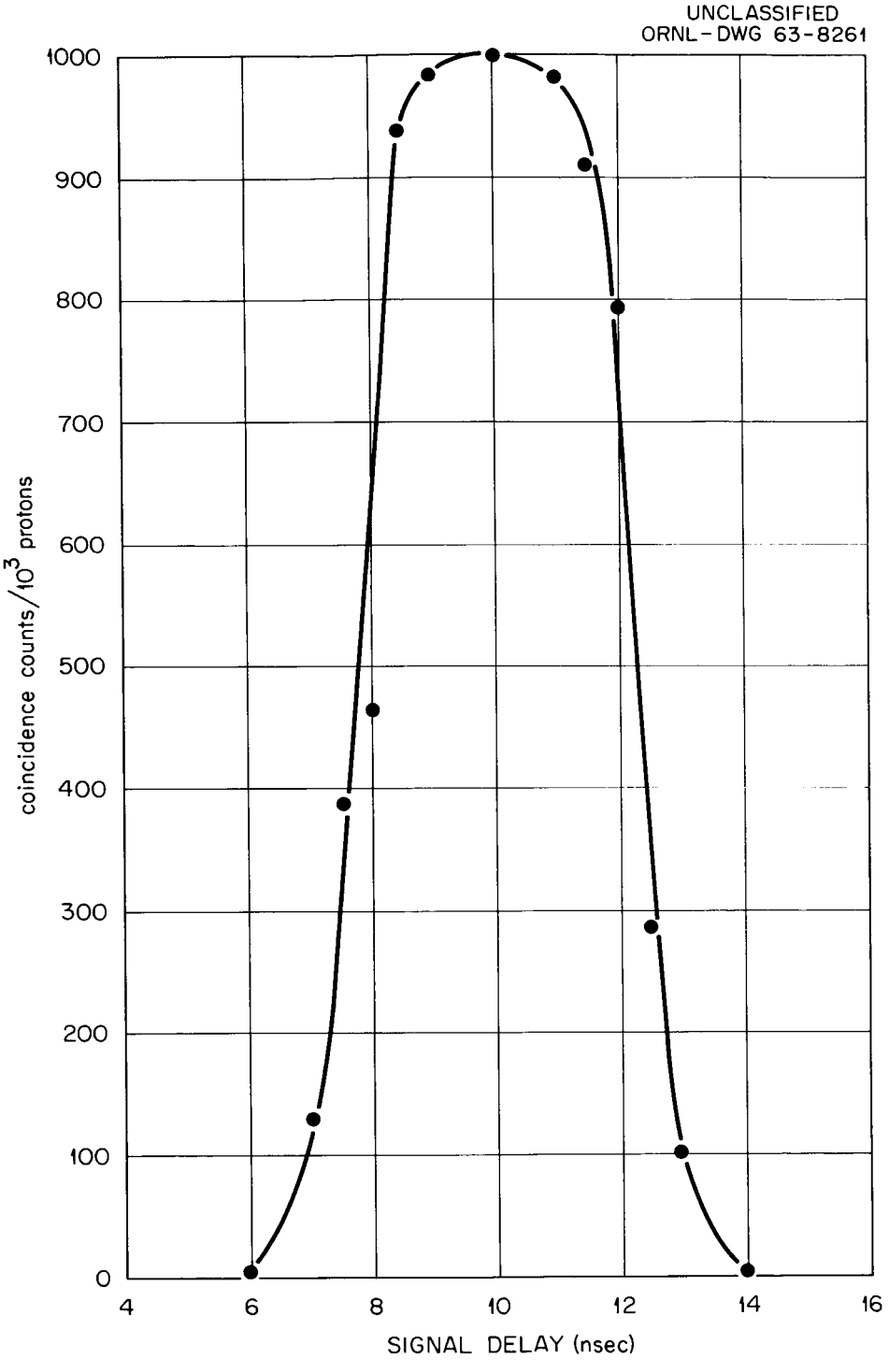

Fig. 18. Delayed Coincidence Curve for the Beam Scintillators. The slopes at the sides of this curve and the null observations 2 standard deviations from its center suggest 100% counting efficiency.

A third difficulty comes in the fact that, especially in the fast scaler systems, grossly incorrect results may be recorded because of failure of the scaler or its driver. For this reason only those sets of counting data were accepted for which at least two (of possible three) fast scaler readings differed by less than 2%. The number of "Stop" signals in the time-to-amplitude converter was also required to agree with the scaler data to within 4%. The dead time in this entirely separate system was imprecisely known, and the apparent discrepancies in this count ranged from 1.5 to 3.5%. The standard error in the fast scaler reading is estimated to be 1.5% based on these selection criteria. This is many times the statistical uncertainty.

A last problem exists because effects of scattering and poor beam focus allow some protons to deposit charge in the ionization chamber without passing through the scintillator system.

Measurements of the space dependence of the beam in the region of the scintillator indicate a beam profile suggestive of multiple scattering. The protons are normally distributed with a standard deviation (vertical and horizontal) of < 0.145 in. This implies that if the beam is centered, less than 0.001% of the unscattered protons miss the 1.5-in.-diam scintillators. The beam would need to be displaced by nearly a centimeter for this "miss" error to reach the 1% level, and photographs indicate a maximum position uncertainty of no more than 0.5 cm.

The material in the ionization chambers, the air between the chambers and the scintillators, and the first scintillator amounts to about 0.25 g/cm^2, so that nuclear reactions and shadow scattering deplete the beam about 0.4%. Coulomb scattering in the aluminum foil of the ionization chambers at an angle large enough to cause protons to miss the scintillators is estimated at only 0.1%.

The Observed Number of Ion Pairs per Proton

Based on the counting and calibration uncertainties discussed above, the observed charge per proton should be reduced by about 0.5% to compensate for coincidence circuit inefficiency, and by an additional 0.5%

to account for scattering losses in the intervening material. However, most of this material was also present during calibration observations using the Faraday cup, so for comparative data the observed ratio should be reduced by only 0.7%. According to the above analysis, the results for each measurement should be good to an uncertainty of about 2%, the greatest contributor being counting errors in the fast scalers. No large scatter among the experimental results would be expected.

The observed results, which did not behave as expected, are summarized in Table 4.

The values in Table 4 reflect several assumptions which require discussion. The standard deviation of the raw observations is a few times greater than what might have been anticipated from known causes, and plots of the time sequence of readings suggest that high or low values occur in bunches. The use of the average reading symbolizes that the systematic errors which caused these discrepancies are unknown in sign, since whenever checked the equipment showed proper calibration. The uncertainty in the observed value was chosen smaller than the standard deviation of the observations but much larger than the usual standard error of the mean of values drawn randomly from a normally distributed sample. The uncertainties analyzed in previous paragraphs were lumped to an estimated 1.5 (ip/proton), but this increment (of doubtful magnitude) does not significantly influence the final error estimates.

The uncertainty in the final result is much larger than should have been observed in an experiment of this type. The inexplicably large range of individual experimental values of (ip/proton) tends to make the quoted results seem unreliable. It is felt that the quoted uncertainty estimates appropriately cover the unreliability experienced.

Discussion and Results

The results of five separate calibrations of the ionization chambers are compared in Table 5. The values of ion pairs per proton obtained by the direct proton counting technique are higher by 1.5 and 1 standard errors than the values obtained with the Faraday cup method for the corresponding run, No. 4. Percentagewise, the differences are 4.2 and 3.3%,

Table 4. Results of Ionization Chamber Calibration by Direct Counting of Protons Responsible for the Measured Charge

	Results (ip/proton)	
	Ionization Chamber No. 1	Ionization Chamber No. 2
Average Raw Value	98.5	82.0
Std. Dev. of Observations	5.8	7.1
Std. Error of Mean (if readings randomly distributed)	0.9	1.3
Estimated Std. Error (considering bunching of readings)	2.	3.
Correction for Scattering and Coincidence Efficiency	-0.6	-0.6
Uncertainty Increment for Other Effects[b]	1.5	1.5
Final Result	87.5 ± 2.5	81.4 ± 3.5

a. A total of 46 observations were made for Ionization Chamber No. 1; a total of 29 for Chamber No. 2.

b. These are the effects described in the text under "Analysis of the Counting Data."

Table 5. Comparison of Results of All Calibration Runs

Run No.	Ion Pairs per Proton		Ratio, IP_1/IP_2
	Chamber No. 1	Chamber No. 2	
1	78.9 ± 0.3	74.6 ± 1.1	1.058
2	78.2 ± 0.5	74.0 ± 1.1	1.057
3	85.3 ± 1.2	76.9 ± 1.4	1.109
4	84.2 ± 1.3	78.8 ± 1.7	1.069
4a[a]	87.5 ± 2.5	81.4 ± 3.5	1.075

a. Calibration by direct counting of protons.

for chambers 1 and 2, respectively. This agreement is encouraging since, to the authors' knowledge, no similar comparison has been reported. Marshall et al.[30] have reported beam measurements, accurate to ±7%, using proton counting techniques, while Koehler[31] has measured the intensity of the Harvard Synchrocyclotron beam to within ±9% using a Faraday cup. Since the experiments using these calibrations all contain other uncertainties at the 5% level, the agreement between the calibrations by the two methods is satisfactory. The similarity of the differences for the two chambers suggests that a systematic error is involved.

It is interesting to note that the measured response of the ionization chambers is in agreement with the calculated response within the errors quoted for each value. Thus, had the beam been monitored using "uncalibrated" ionization chambers, the error introduced would have been of the same order of magnitude as the other uncertainties in the spectral measurements.

Acknowledgments

It is a pleasure to acknowledge the efforts of the people whose advice and assistance aided these measurements. Among these were Dr. A. M. Koehler of the Harvard University Synchrocyclotron staff, whose contributions included equipment and many helpful suggestions concerning calibration techniques. The assistance of R. K. Abele, W. T. Clay, N. W. Hill, and R. J. Scroggs, all of the ORNL Instrumentation and Controls Division, has been footnoted in the text, as has that of R. L. Cowperthwaite of the Neutron Physics Division. The authors are also grateful to the members of the Space Team who helped with these measurements. They include T. V. Blosser, W. R. Burrus, W. A. Gibson, T. A. Love, F. C. Maienschein, and W. Zobel.

---

30. J. Marshall et al., Phys. Rev. 92, 834 (1955).

31. A. M. Koehler, Harvard University, private communication.

Appendix. Calibration of Constant Current Sources

A constant current source is shown schematically in Fig. 19. For Source No. 1 the voltage E was 125 V, while for Source No. 2 it was 1.25 V. Both voltages were supplied by mercury cells because of their stability over their characteristically long lifetimes. The resistance R had a value of 10^{12} ($\pm$10%) Ω for both sources. At the terminal marked "i," the current is given by: $i = E/R$. The BNC-type connectors used at the "E" and "i" terminals had a leakage resistance from the center pin to ground of 10^{13} Ω or more.

The current source calibration circuit is shown in Fig. 20. A precise current, i_2, was supplied by the Rubicon potentiometer, calibrated against a standard cell (standardized by NBS), and a precision resistance, R_k. The resistance consisted of four 25-Meg resistors having a guaranteed tolerance of $\pm$0.1%. The voltage E_k was adjusted with the potentiometer until $E_k/R_k = i_2 = i_1$, determined by reading a null condition on a picoammeter. With this technique the working voltage, E_k, could be adjusted to null the unknown current from the source being standardized to an accuracy of a few parts in ten thousand. When the null condition was achieved, the ratio E_k/E_R gave the value of the source current, i_1. This is valid provided that the meter current, i_3, can be neglected relative to i_1 and provided that the allowable i_3 yields an observable deflection on the meter.

The ratio E_k/E_R was known to at least 0.1%, and if the sensitivity of the meter was such that the uncertainty in i_3 was a few parts in 10^{-14} A, then i_2 was measured to within 0.2%.

By using this technique, Current Source No. 1 was determined as 1.34($\pm$0.2%) x 10^{-10} A. The larger error ($\pm$1%) quoted in the text allows for any stray ion current or variation in cell voltage from its value at the time of calibration.

The vibrating-reed electrometer, calibrated against Source No. 1, was used to determine the value of Current Source No. 2 as 1.42 ($\pm$3%) x 10^{-12} A, the $\pm$3% tolerance accounting for all possible errors due to leakage, ion currents, or battery voltage.

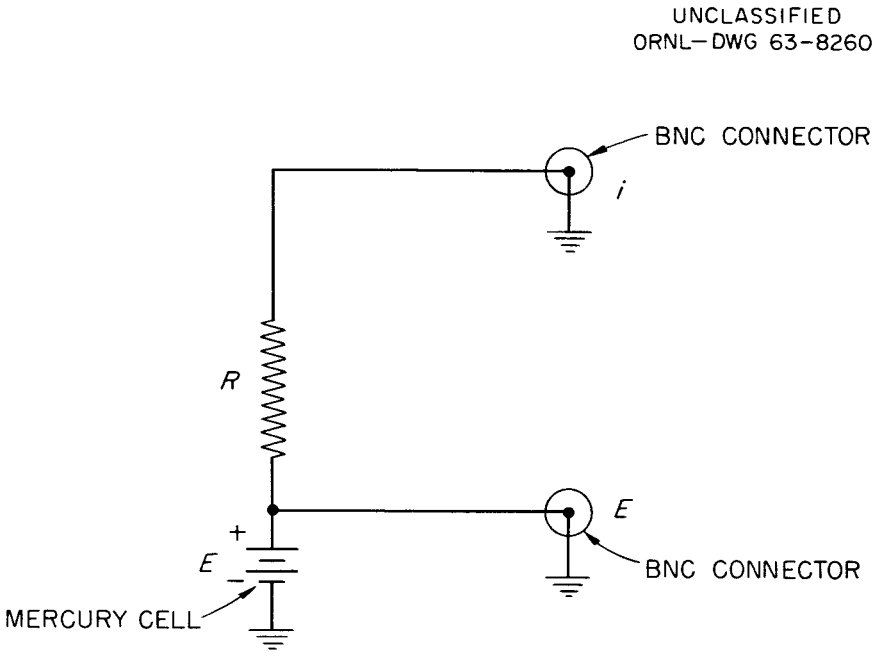

Fig. 19. Schematic Diagram of Constant-Current Source.

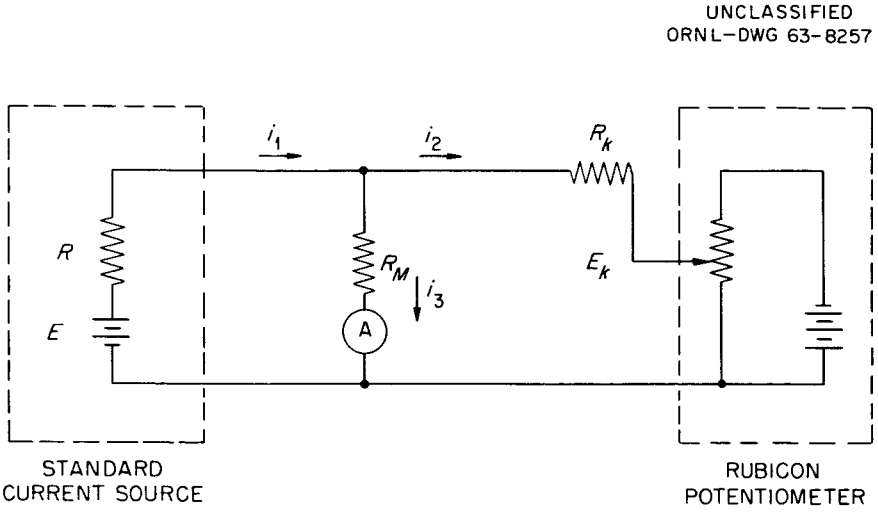

Fig. 20. Schematic Diagram of Calibration Circuit.

ORNL-3505
UC-34 — Physics
TID-4500 (27th ed.)

INTERNAL DISTRIBUTION

1. Biology Library
2-4. Central Research Library
5. Reactor Division Library
6-7. ORNL — Y-12 Technical Library Document Reference Section
8-57. Laboratory Records Department
58. Laboratory Records, ORNL R.C.
59. J. A. Auxier
60. R. Bender
61. E. P. Blizard
62. L. Blumberg
63. H. R. Brashear
64. R. D. Birkhoff
65. R. Burrus
66. W. T. Clay
67. R. M. Freestone, Jr.
68. W. A. Gibson
69. M. L. Halbert
70. F. F. Haywood
71. F. T. Howard
72. W. H. Jordan
73. C. E. Larson
74. F. C. Maienschein
75. W. F. Mruk
76-78. R. W. Peelle
79. J. J. Pinajian
80-99. R. T. Santoro
100. M. J. Skinner
101. J. A. Swartout
102. A. M. Weinberg
103. L. V. Weston
104. W. H. White, Jr.
105. W. Zobel
106. A. Zucker
107. R. A. Charpie (consultant)
108. P. F. Gast (consultant)
109. M. L. Goldberger (consultant)
110. R. F. Taschek (consultant)
111. T. J. Thompson (consultant)

EXTERNAL DISTRIBUTION

112. G. W. Crawford, Physics Department, Southern Methodist University, Dallas, Texas
113. A. M. Koehler, Physics Department, Harvard University, Cambridge, Massachusetts
114. T. Knasel, Physics Department, Harvard University, Cambridge, Massachusetts
115. W. M. Preston, Physics Department, Harvard University, Cambridge, Massachusetts
116. J. E. Duberg, NASA, Langley Field, Virginia
117. Trutz Foelsche, NASA, Langley Research Center, Hampton, Virginia
118. W. C. Hulten, NASA - IRD, Langley Research Center, Hampton, Virginia
119. L. F. Vosteen, NASA, Langley Research Center, Hampton, Virginia
120. W. L. Gill, NASA, Manned Spacecraft Center, Houston, Texas
121. R. H. Steelle, NASA, Manned Spacecraft Center, Houston, Texas
122. Evalyn Repplinger, Crew Systems Division, Houston, Texas
123. W. N. Hess, NASA, Goddard Space Flight Center, Greenbelt, Maryland
124. H. E. Stern (M-RP-N), NASA, George C. Marshall Space Flight Center, Huntsville, Alabama
125. Frank Voorhis, USAF (MC), OART/RBH, NASA, Washington, D.C.
126. J. W. Keller, NASA Headquarters, Washington, D.C.
127. Jerry Modisette, Manned Spacecraft Center, Houston, Texas

128. Jim Johnson, LTV Research Center, Dallas, Texas
129. Lt. Duane Adams, Air Force Weapons Laboratory, WLRB-1, Kirtland Air Force Base, New Mexico
130. Lt. Col. Edward Harney, Air Force Space Systems Division, SSTA, Air Force Unit Post Office, Los Angeles, California
131-133. Aerospace Corporation, 2400 El Segundo Blvd., El Segundo, California (1 copy each to F. L. Keller, Stan Freden, and Robert Pruett)
134. George Joanou, General Atomic, San Diego, California
135. G. F. Pieper, NASA Headquarters, Washington, D.C.
136. Arthur Reetz, NASA Headquarters, Washington, D.C.
137. R. C. Good, Jr., General Electric Company, Philadelphia, Pennsylvania
138. R. T. Siegel, College of William and Mary, Williamsburg, Virginia
139. K. Ziock, University of Virginia, Charlottesville, Virginia
140. Jerry Speakman, 6570 AMRL (MRBBR), Wright-Patterson Air Force Base, Ohio
141. T. J. McGuire, ASD(ASRSSV-e), Shielding Research Reports, Wright-Patterson Air Force Base, Ohio
142. Loren Pittman, 6570 AMRL (MRBBR), Wright-Patterson Air Force Base, Ohio
143. Capt. R. F. Cooper, ASRPE-20, Wright-Patterson Air Force Base, Ohio
144. C. A. Dempsey, 6570 AMRL, Wright-Patterson Air Force Base, Ohio
145. R. E. Fortney, Northrop Space Laboratories, Hawthorne, California
146. M. C. Chapman, Northrop Space Laboratories, Hawthorne, California
147. S. H. Levine, Northrop Space Laboratories, Hawthorne, California
148. L. W. McCleary, North American Aviation, Inc., Downey, California
149. G. E. Laubaugh, North American Aviation, Inc., Downey, California
150. Frederick Raymes, North American Aviation, Inc., Downey, California
151. M. R. Kinsler, North American Aviation, Inc., Downey, California
152. E. R. Beever, North American Aviation, Inc., Downey, California
153. T. J. Rock, General Dynamics, Fort Worth, Texas
154. C. F. Johnson, General Dynamics, Fort Worth, Texas
155. T. R. Strayhorn, General Dynamics, Fort Worth, Texas
156. G. T. Western, General Dynamics, Fort Worth, Texas
157. R. A. Miller, General Dynamics, Fort Worth, Texas
158. T. W. De Vries, General Dynamics, Fort Worth, Texas
159. E. C. Kidd, General Dynamics, Fort Worth, Texas
160. D. H. Robey, General Dynamics/Astronautics, San Diego, California
161. Sidney Russak, The Martin Company, Baltimore, Maryland
162. Ed Divita, 1504 Doxbury Road, Towson, Maryland
163. I. M. Karp, Lewis Research Center, Cleveland, Ohio
164. R. I. Hildebrand, Lewis Research Center, Cleveland, Ohio
165. R. V. Meghreblian, Jet Propulsion Laboratory, Pasadena, California
166. R. J. Mackin, Jr., Jet Propulsion Laboratory, Pasadena, California
167. F. Felberg, Jet Propulsion Laboratory, Pasadena, California
168. D. F. Spencer, Jet Propulsion Laboratory, Pasadena, California
169. D. L. Dye, Boeing Aircraft Company, Seattle, Washington

170. Maurice Wilkinson, Boeing Aircraft Company, Seattle, Washington
171. J. C. Noyes, Boeing Scientific Research Laboratories, Seattle, Washington
172. J. F. Kenney, Boeing Scientific Research Laboratories, Seattle, Washington
173. Maynard Pearson, Boeing Aircraft Company, Seattle, Washington
174. Brian Mar, Boeing Aircraft Company, Seattle, Washington
175. Lt. Col. R. G. Allen, Jr., USAF Aerospace Medical Center, Brooks Air Force Base, Texas
176. Col. J. E. Pickering, USAF Aerospace Medical Center, Brooks Air Force Base, Texas
177. W. M. Schofield, Advanced Research Corporation, Atlanta, Georgia
178. E. C. Smith, Advanced Research Corporation, Atlanta, Georgia
179. Wade Patterson, University of California, Lawrence Radiation Laboratory, Berkeley, California
180. Cornelius Tobias, University of California, Lawrence Radiation Laboratory, Berkeley, California
181. M. J. Berger, National Bureau of Standards, Washington, D.C.
182. H. J. Schulte, Bellcomm, Inc., Washington, D.C.
183. Phil Mittleman, United Nuclear Corporation, White Plaines, New York
184. Sol Krasner, Office of Naval Research, Washington, D.C.
185. W. H. Langham, Los Alamos Scientific Laboratory, Los Alamos, New Mexico
186. M. A. Van Dilla, Los Alamos Scientific Laboratory, Los Alamos, New Mexico
187. G. A. Whan, University of New Mexico, Albuquerque, New Mexico
188. D. W. Drawbaugh, Westinghouse Electric Company, Pittsburgh, Pennsylvania
189. E. M. Finkelman, Grumman Aircraft, Bethpage, New York
190. R. V. Glowszwski, McDonnell Aircraft, St. Louis, Missouri
191. R. A. Glass, Lockheed Missiles and Space Company, Palo Alto, California
192. S. P. Shen, New York University, New York, New York
193. J. P. Neissel, General Electric Company, Schenectady, New York
194. R. L. Harvey, General Electric Company, San Jose, California
195. David Langford, Pratt and Whitney Aircraft, East Hartford, Connecticut
196. C. W. Hill, Lockheed-Georgia Company, Marietta, Georgia
197. C. K. Bauer, Lockheed-Georgia Company, Marietta, Georgia
198. K. D. George, Pictinny Arsenal, Dover, New Jersey
199. R. B. Curtis, University of Indiana, Bloomington, Indiana
200. H. J. Schaefer, U.S. Naval School of Aviation Medicine, Pensacola, Florida
201. William Steigelmann, Kuljian Corporation, Philadelphia, Pennsylvania
202. G. P. Wachtell, Franklin Institute, Philadelphia, Pennsylvania
203. Keith More, Bendix Systems Division, Ann Arbor, Michigan
204. L. R. Lewis, Bendix Systems Division, Ann Arbor, Michigan
205. T. H. Colvin, Bendix Systems Division, Ann Arbor, Michigan
206. Borje Larsson, The Gustaf Werner Institute, University of Uppsala, Uppsala, Sweden

207. Martin Leimdorfer, Research Institute of National Defense, FOA4, Stockholm 80, Sweden
208. Richard Madey, Republic Aviation Corporation, Farmingdale, Long Island, New York
209. F. E. Schwamb, Applied Physics Research, Republic Aviation Corporation, Farmingdale, Long Island, New York
210. C. D. Zerby, Union Carbide Research Institute, Tarrytown, New York
211. Fred Casal, NASA Headquarters, Washington, D.C.
212. V. B. Bhanot, Physics Department, Panjab University, Chandigarh-3, India
213. Jacobo Rapaport, University of Chile, Box 2777, Institute of Science, Santiago, Chile
214. Research and Development Division, AEC, ORO
215-849. Given distribution as shown in TID-4500 (27th ed.) under Physics category (75 copies – OTS)

Errata: ORNL-3505

MEASUREMENT OF THE INTENSITY OF THE PROTON BEAM OF THE HARVARD UNIVERSITY SYNCHROCYCLOTRON FOR ENERGY-SPECTRAL MEASUREMENTS OF NUCLEAR SECONDARIES*

Note: These errata are printed on gummed paper so that they can be cut apart and glued directly into the report.

Page 2 - Footnote 5

5. Designed and built by R. K. Abele, Instrumentation and Controls Division. Construction details are given in Drawing A-2540.

Page 4 - Figure 2 - In place of Aluminized Mylar Window (2 places) it should read 2-mil-thick aluminum foil.

2-mil-thick aluminum foil window	2-mil-thick aluminum foil window